Dissertation

The role of ABCG2 transporter in Pulmonary Hypertension (PH)

submitted by

Bence M. NAGY

for the Academic Degree of

Doctor of Philosophy (PhD)

at the

Medical University of Graz

Department of Internal Medicine

Division of Pulmonology

under the Supervision of

Prof. Dr. Horst OLSCHEWSKI

2017

Statutory Declaration

I hereby declare that this dissertation is my own original work and that I have fully acknowledged by name all of those individuals and organisations that have contributed to the research for this dissertation. Due acknowledgement has been made in the text to all other material used. Throughout this dissertation and in all related publications I followed the “Standards of Good Scientific Practice and Ombuds Committee at the Medical University of Graz”.

22.03.2017

Bence M.Nagy

Acknowledgements

This PhD dissertation is the result of work and study has been carried out at the Medical University of Graz in the Center for Medical Research (ZMF).

First and foremost, I would like to thank to Prof. Horst Olschewski and Prof. Andrea Olschewski for providing me the opportunity and trust to be a member of their scientific group and to obtain my PhD degree in their laboratory. I believe, their knowledge and kind support significantly contributed not only to my scientific- but to my personal development as well. I would really like to thank Dr. Chandran Nagaraj for devoting his time and patience during these years, motivating me daily to improve my knowledge and move my career forward. Without him, this PhD dissertation may not have been written. Special thanks to Dr. Valentina Biasin for standing by me and giving me valuable advices in the most crucial times. I would like to express my gratitude to Dr. Edit Pollák for her efforts to keeping me on the right track and not letting me drifting away many-many years ago. Special thanks to Dr. Antal Tapodi, Dr. Balázs Veres, and Dr. Péter Jakus for not giving up on me and introducing me into the incredible world of science, in the beginning of my career. I also wish to thank Elisabeth Blanz, Elisabeth Poellitzer, Sabine Halsegger and Simone Tischler for their hard and excellent work in any projects we were/are working on. I also would like to thank all my colleagues in the Ludwig Boltzmann Institute for Lung Vascular Research for their valuable advices and for the fruitful discussions.

Beside their scientific impact on me, majority of the above mentioned persons have honoured me with their friendship for which I will always be grateful most, thank You.
Last, but not least, I would like to thank to my family for making it possible for me to follow my ambitions, despite all the sacrifices they had to make for this.

Table of Contents

Abbreviations and Definitions

ABC transporter	ATP-binding cassette transporter
Akt	Protein Kinase B
AML	Acute Myeloid Leukemia
BBB	Blood Brain Barrier
BCRP	Breast Cancer Resistance Protein
BW	Body Weight
cAMP	Cyclic adenosine monophosphate
CFTR	Cystic Fibrosis Transmembrane Conductance
cGMP	Cyclic guanosine monophosphate
CO	Cardiac output
Col1A1	Collagen type I alpha 1
EC	Endothelial Cell
ECM	Extracellular matrix
EDP	End Diastolic Pressure
EGF	Epidermal Growth Factor
ERK	Extracellular Signal-Regulated Kinase
FTC	Fumitremorgin C
GAPDH	Glyceraldehyde-3-Phosphate Dehydrogenase
Hct	Hematocrit
HIF-1	Hypoxia Inducible Factor 1
HMVEC	Human Microvascular Endothelial Cells
HRE	Hypoxia Response Element
IPAH	Idiopathic Pulmonary Arterial Hypertension
KO	Knock Out
LV	Left Ventricle of the heart
LVEDP	Left Ventricular End Diastolic Pressure
LVSP	Left Ventricular Systolic pressure
MDR	Multidrug Resistance
MI	Myocardial Infarction
mPAP	Mean Pulmonary Artery Pressure
MRP	Multidrug Resistant Protein
MSC	Mesenchymal Stem Cells
PA	Pulmonary artery
PAEC	Pulmonary Artery Endothelial Cells
PAH	Pulmonary Arterial Hypertension

PASMC	Pulmonary Artery Smooth Muscle Cells
PAWP	Pulmonary Artery Wedge Pressure
PBS	Phosphate Buffered Saline
PDE	phosphodiesterase
PDGF	Platelet Derived Growth Factor
Pgp	P-glycoprotein
PH	Pulmonary Hypertension
PPAR	Peroxisome Proliferator-Activated Receptor
PPIX	Protoporphyrin IX
PVR	Pulmonary vascular resistance
ROS	Reactive oxygen species
RV	Right Ventricle of the heart
RVEDP	Right Ventricular End Diastolic Pressure
RVSP	Right Ventricular Systolic pressure
SBP	Systemic Blood Pressure
siRNA	small interfering RNA
SP	Side Population
TAC	Transverse Aortic Constriction
TIMP	Tissue Inhibitor of Metalloproteinase
TSS	Transcription Start Site
WHO	World Health Organization
WT	Wild Type

Abstract in German

Der Adenosin triphosphate-binding cassette transporter (ABCG2) schützt Krebszellen vor Chemotherapie und vor durch erhöhten Druck induzierter Dysfunktion des Ventrikels. Der Transporter ist im Myokardium von Patienten mit Herzfehlern hochreguliert und reduziert durch Hypoxie hervorgerufene Metaboliten. Um die Relevanz von ABCG2 für die Lungen- und Herzfunktion sowie Lungen- und Herzstruktur unter chronischer Hypoxie zu untersuchen, wurden in dieser Studie ABCG2 Knockout (KO) Mäuse verwendet und mit weiteren Experimenten an primären menschlichen Lungenzellen ergänzt.

Wir konnten zeigen, dass ABCG2 in den Lungengefäßen vorkommt und deren Expression in Lungen von Patienten mit Idiopathischem Lungenhochdruck (IPAH) erhöht ist. In gesunden Glattmuskelzellen der Lunge (PASMC) konnte eine Erhöhung der ABCG2 Expression durch Stimulation mit Platelate derived growth factor (PDGF) induziert werden. Inhibierung des Transporters führte zu einer verringerten Proliferation dieser Zellen. Wider erwarten kam es in ABCG2 KO Mäuse nach 4 wöchiger Hypoxie-Behandlung nicht zu einer Reduzierung des Gefäßumbau, jedoch wiesen die KO Mäuse in Hypoxie im Vergleich zu Wildttyp Mäusen eine verstärkte rechts (RV) und Links (LV) ventrikuläre diastolische Dysfunktion auf, manifestiert durch einen erhöhten end-diastolischen Druck und Fibrose im Myokardium ohne dabei die systolische Funktion zu beeinträchtigen. Die Hypoxie-Behandlung führte in ABCG2 KO Mäusen zwar zu einem Umbau des Ventrikels, jedoch blieb die Dichte der Kapillare in Normoxie sowie Hypoxie unverändert. Passend dazu zeigten Fibroblasten des Herzens von ABCG2 KO Mäusen sowie vom Menschen in Hypoxie eine erhöhte Produktion von Kollagen.

Zusammenfassend konnten wir zeigen, dass speziell unter Hypoxie, der Verlust von ABCG2 zu einer bi-ventrikulären Fibrose mit diastolischer Dysfunktion führt, jedoch dies keinen Effekt auf den Lungenhochdruck, RV Nachlast und Dichte der Kapillaren hat. Unsere Studie hinterfragt hiermit die Anwendung von ABCG2 Inhibitoren in Krebspatienten, im speziellen bei denen die hypoxämisch sind oder unter ischämischen Herzerkrankungen leiden, da diese Inhibitoren möglicherweise zu einer medikamentös induzierter Kardiotoxizität führen können.

Abstract in English

The adenosine triphosphate-binding cassette (ABC)G2 transporter protects cancer cells from chemotherapy but it also protects from pressure overload-induced ventricular dysfunction. It is upregulated in the myocardium of heart failure patients and is clearing hypoxia-induced intracellular metabolites. This study employs ABCG2 knockout (KO) mice to elucidate the relevance of ABCG2 for pulmonary- and cardiac function and structure in chronic hypoxia, and uses human explanted tissues and primary cells to investigate the role of ABCG2 in humans.

Our results showed that ABCG2 was present in the main cellular components of the human lung vasculature, and it was upregulated in patients with idiopathic pulmonary hypertension (IPAH). The expression of ABCG2 in pulmonary arterial smooth muscle cells (PASMC) was regulated by platelet derived growth factor (PDGF), and inhibition of the transporter abolished the proliferation of these cells. However, when ABCG2 KO and control mice were subjected to 4 weeks normoxia or hypoxia, there was no difference in hypoxia-induced pulmonary hypertension or vascular remodelling between ABCG2 KO and wild type mice. On the other hand, in hypoxia, KO mice showed pronounced right- (RV) and left (LV) ventricular diastolic dysfunction, manifested by an increase in end-diastolic pressure and myocardial fibrosis, whereas systolic function was preserved. Despite increased ventricular remodelling, capillary density was unaffected by ABCG2 and by hypoxia. In line with these observations ABCG2-deficient mouse and human cardiac fibroblasts showed increased collagen production in hypoxia.

As a conclusion, we provide evidence that particularly under hypoxia, loss of ABCG2 leads to biventricular fibrosis with diastolic dysfunction, although it does not affect pulmonary hypertension, RV afterload and capillary density. Our study raises concerns regarding the use of ABCG2 inhibitors in cancer patients especially with hypoxemia or ischemic heart disease, as it might cause drug-induced cardiotoxicity.

Introduction

Pulmonary Hypertension

Pulmonary arterial hypertension (PAH) is an enigmatic disease characterized by progressive increase in pulmonary vascular resistance leading to right ventricular overload, right heart failure and eventually premature death. PAH may be idiopathic or hereditary or related to other diseases, including connective tissue disease, chronic liver disease and congenital heart disease. Although PAH is a rare disease with 15-50 cases/million people, in certain risk groups (HIV (1), systemic sclerosis (2,3), sickle cell disease (4)) the incidence of PAH is substantially higher(5). The idiopathic form of pulmonary arterial hypertension (IPAH) has a prevalence of 1-2 cases/million and is about three-times more common in young women than in young men (6,7). Due to the non-specific nature of symptoms – which can occur at any time of life-, the mean age at diagnosis is around 40-70 years. At diagnosis, most patients present with an advanced stage of disease (8).

The elevated resistance of the lung vasculature is the reflection of vasoconstriction and/or the remodelling of pulmonary arteries (PA), which are hallmarks of PAH. There are different concepts attempting to explain the pathogenesis of PAH and each of them has certain relevance for the development of the disease (9-11). The imbalance of endothelial function favors vascular mitogenesis, thrombosis and, more importantly, plays a regulatory role in chronic vasoconstriction (12). On the other hand, there is evidence showing that pulmonary arterial smooth muscle cells (PASMC) can directly cause vasoconstriction via mitochondrial-derived reactive oxygen species (ROS), impaired Ca^{2+} handling, or through the Rho-kinase pathway (13). The remodelling of PAs might occur due to impaired apoptosis, excess proliferation, or an altered metabolism of vascular cells, indicating analogies with tumorigenic processes (14). Additionally, these pathological alterations are more presumable if mutation of certain genes (BMPR2, KCNK3, CAV1, EIF2AK4) occur (15).

The treatment of PAH currently address vasoconstriction with the use of prostanoids (16,17), endothelin receptor blockers (18,19), and/or phosphodiesterase (PDE) inhibitors (20). High doses of L-type calcium channel blockers are effective as well, however, only in a small

subgroup of patients who present with a strong vasodilator response to NO or other strong pulmonary vasodilators (21). Until recently, most patients received anticoagulants to prevent in situ thrombosis in the pulmonary arteries. Many patients profit from diuretics, particularly aldosterone antagonists.

Despite all these advances, PAH therapy remains a palliative therapy; and the pulmonary vascular resistance (PVR) continues to increase in the majority of patients. The right ventricle (RV) has the ability to adapt to the progressively increasing afterload and develops an increasing myocardial mass (hypertrophy). However, at a certain point of time, the RV is unable to cope with the elevated afterload and fails. If all available targeted PAH therapies were unable to prevent this course, the patient may be a candidate for lung transplantation and/or atrial septostomy (22). Taken together, although an alteration in the lung vasculature is the primary cause of pulmonary hypertension, yet the sustained adaptive capacity of the RV is the main determinant of the patient's survival (23).

In the last few years the RV is receiving increasing interest in the PH research field. Despite this, still little is known about the mechanisms of RV adaptation and failure or about the direct effects of PH therapy on the heart (24-26). This emphasizes the importance of a continued effort to decipher the pathobiological processes underlying PH, with special attention towards the right ventricle.

ABC Transporters

Previous studies have shown the relevance of channels and membrane transporters in PH, highlighting their crucial role in the pathogenesis of the disease (27-29). However, the contribution of a large family of transporters, -namely ABC transporters- remains unexplored. ATP-binding cassette (ABC) transporters are cell membrane proteins that translocate a plethora of different substrates across biological membranes, in an ATP-dependent manner. These substrates can be exogenous drugs, toxins, metabolic products, nutrients, xenobiotics or any harmful agents (30). Therefore these transporters are crucial for the majority of physiological, pharmacological, and pathological processes. In humans, there are 48 ABC transporters, divided into 7 distinct subfamilies based on their gene structure similarities and sequence homology: ABC A, -B, -C, -D, -E, -F, -G (31).

Functional ABC proteins typically contain at least one nucleotide (ATP)-binding domain (NBD) and two-to several transmembrane (TM) domains. The TM domains form the structural unit of the transporter, containing 6-11 membrane spanning α-helices and provide the specificity for the substrate. The NBDs are located in the cytoplasm and transfer the energy to transport the substrate across the membrane. ABC transporters are mostly unidirectional. In bacteria, they are predominantly involved in the import of essential compounds that cannot be obtained by diffusion (sugars, vitamins, metal ions, etc.) into the cell. In eukaryotes, most ABC genes move compounds from the cytoplasm to the outside of the cell or into an intracellular compartment (ER, peroxisome, mitochondria) (31).

The expression profile of the ABC transporter family has been investigated in 20 different human tissues and showed that organs involved in barrier function (lung, intestine), or secretory function (prostate, adrenal gland) express more of the transporters (32).

Three ABC transporters are known to play an important role in lung physiology, as disturbances in their function lead to well-known pulmonary diseases. Mutations in the cystic fibrosis transmembrane conductance regulator (CFTR) gene (ABCC7) can cause cystic fibrosis; and dysfunction of ABCA1 and ABCA3 are responsible for Tangier disease and fatal surfactant deficiency, respectively (33). Besides this, the prominent expression of ABCB1 and ABCC1 in the human lung suggests that these latter transporters may also be pivotal in the protection

against endogenous or exogenous toxic compounds entering the lung (34). More importantly, a recent study has shown that the expression of multidrug resistance protein (MRP)4 (ABCC4) was increased in pulmonary arteries of IPAH patients, as well as in an animal model of the disease. Furthermore, ABCC4 KO mice were protected from the development of hypoxia-induced PH (35).

ABCG2

ABCG2 is one of the five G subfamily members of the human ABC protein superfamily, along with ABCG1, ABCG4, ABCG5 and ABCG8. All members of this subfamily are half-transporters, therefore thought to function either as homo- or heterodimers, or possibly even as larger oligomeric structures (36). Another speciality of the G subfamily of ABC transporters is that the nucleotide-binding domain (NBD) is not C-, but N-terminal to the transmembrane domain, whereas the opposite is true for other ABC transporters.

Previous studies have shown apical localisation of ABCG2 in epithelial cells of the intestine, gallbladder, cervix, alveolar pneumocytes, hepatocytes or gland cells, but it has also been detected in placental trophoblasts or capillaries of different origin (37-40). Since the *ABCG2* gene was first isolated from a breast cancer cell line, the transporter was originally termed as breast cancer resistance protein (Bcrp). The *ABCG2* gene is localised on chromosome 4 and includes 15 introns and 16 exons. The transcription start site (TSS) was found 529 bp upstream from the border of exons 1 and 2. Its promoter region was identified between nucleotides -300 and -50 relative to the TSS (41). Hypoxia Inducible Factor (HIF1) is able to bind to the hypoxia response element (HRE) of the *ABCG2* promoter, therefore it can regulate *ABCG2* expression under hypoxia (42). In hypoxic conditions, the synthesis of heme is inversely proportional to the partial pressure of oxygen through the HIF1 pathway, depending on the oxygen concentration (43). However, accumulation of intracellular heme, leads to iron overload and consequently elevated production of detrimental ROS (44). ABCG2 can actively efflux heme, therefore enhance survival of these cells in hypoxia (42).

Growth factors – like epidermal growth factor (EGF) - are likely to be involved in ABCG2 gene regulation as well (45). The peroxisome proliferator-activated receptor (PPAR) also activates the *ABCG2* mRNA (46), just like progesterone and estradiol (47-49). Several splice variants of

ABCG2 have been described before, differing from each other at exon 1. In humans, the expression of these variants differs between different tissues, suggesting a tissue-specific alternative promoter usage for transcriptional regulation (45).

Since ABCG2 has a primary role in cell-defense against harmful agents, its substrates cover a broad spectrum of molecules with both exogenous and endogenous origin. Amongst others, the substrates of ABCG2 comprise natural compounds and toxins, anticancer drugs, fluorescent dyes, or antiobiotics (36,50) (*Table 1*). ABCG2 can largely influence the pharmacokinetics of many drugs and their metabolites, by facilitating their excretion and limiting their uptake (51).

The ability of a cell to actively extrude a wide range of substrates, gives the advantage to acquire and maintain a phenotype which differs from the surrounding cells. For instance, the fascinating property of stem cells to sustain pluripotency is due to their high expression of ABCG2 (52). Increased ABCG2 expression enhances the proliferative capacity of side population (SP) stem cells, whereas lack of ABCG2 impairs their expandibility (53). Loss of ABCG2 results in a decrease in SP stem cell numbers, because these cells are more sensitive to cytotoxic compounds, confirming the physiological protective function of ABCG2 in stem cells (54,55). Any disturbance in ABCG2-expressing stem cell function results in a pathological alteration in pulmonary tissue structure (56).

As their main role is detoxification, several ABC transporters have been found to be highly expressed in cancer cell lines cultured under selective pressure. Multidrug resistency (MDR) means that cancer cells become resistant to chemotherapeutic agents, eventually leading to the failure of cancer treatment in patients. The most common mechanism of resistance is the active efflux of drugs by ABC transporters (57).

Table 1. ABCG2 substrates (Generated from data, published in references (36, 50))

Anthracyclines (Topoisomerase II inhibitors)
- Epirubicin
- Daunorubicin
- Pirarubicin
- Doxobucincin

Antimetabolites
- 5-fluorouracil
- Cladribine, CdAMP
- MTX, MTX triglutamate, MTX diglutamate
- Piritrexim , metoprine, trimetrexatte, pyrimethamine
- Tomudex, GW1843

Camptothecin analogs (Topoisomerase I inhibitors)
- 9-aminocamptothecin
- BN80915
- Belotecan
- DX-8951f
- CPT-11
- Gimatecan
- Homocamptothecins
- NX211
- SN-38
- Topotecan

Fluorescent dyes
- BODIPY-FL-dihydropyridine
- BODIPY-prazosin
- Cholyl-L-lysyl-fluorescein
- D-luciferin
- Hoechst 33342
- Lysotracker green
- Rhodamine 123

Natural compounds and toxins
- Folic acid
- Genistein
- Glutathione
- Riboflavin
- Sphingosine 1-phosphate
- PhIP
- PPIX
- Urate
- Vitamin K3, plumbagin

Photosensitizers
- 5-aminolevulinic acid
- Chlorine E6
- HPPH
- Pheophorbide a
- Phytoporphyrin
- Pyropheophorbide a methyl ester

Sufate and glucuronide conjugates of xenobiotics
- [14C]4-methylumbelliferone glucuronide
- 17beta-estradiol sulfate
- [3H]17beta-estradiol-17beta-D-glucuronide
- 3-O-sulfate conjugate of 17alpha-ethinylestradiol
- 4[35S]-methylumbelliferone sulfate
- BP-3-sulfate and BP-3-glucuronide
- DHEAS
- E3040 sulfate
- Estrone 3-sulfate
- Phenolic MPA glucuronide
- SN-38-glucuronide
- Troglitazone sulfate

Topoisomerase inhibitors
- Becatecarin
- Bisantrene
- Etoposide
- J-107088, NB-506
- Mitoxantrone

Tyrosine kinase inhibitors
- CI1033
- CP-724,714
- Dasatinib
- Erlotinib
- Gefitinib
- Nilotinib
- Sorafenib
- Symadex
- Tandutinib
- Vandetanib

Other anticancer drugs
- Bicalutamide
- Flavopiridol
- JNJ-7706621
- NSC73306
- TH-337
- Phenethyl isothiocyanate

Others
- Albendazole suloxide and oxfendazole
- Amyloid-beta
- [(3)H]azidopine, IAAP
- Ciprofloxacin,enrofloxacin, norfloxacin, ulifloxacin, grepafloxacin,
- Cimetidine
- Dipyridamole
- Diclofenac
- Befloxatone
- Sulfasalazine
- Zidovudine
- Pitavastatin
- Nifedipine, nicardipine, nitrendipine
- Hesperetin conjugates
- Erythromycin
- Ganciclovir
- ME3277
- Olmesartan medoxomil
- Zoledronic acid
- Nitrofurantoin
- Leflunomide and A771726
- Glyburide
- Prazosin
- Kaempferol
- Moxidectin
- Rosuvastatin
- Lamivudine
- Riluzole

Studies from the cancer field have consistently shown that in most cultured cancer cells, MDR involves ABCB1, ABCC1 or ABCG2 (58). Overexpression of ABCG2 has been found in many cancer cell lines derived from different tumor types including colon cancer (59,60), small cell lung cancer (61), non- small cell lung cancer (62), ovarian cancer (63), gastric carcinoma (64), multiple myeloma (65) or hepatocyte carcinoma (66). ABCG2 is further important due to its expression in the blood-organ barrier, where it significantly limits the penetration of its substrates (including anticancer drugs) into these tissues (51,67-69).

Drug resistancy is obviously a major obstacle in cancer therapy. The potential of ABCG2 to mediate MDR has generated great interest in developing relevant compounds inhibiting its function and reversing acquired drug resistancy (36,51,70,71) (*Table 2*). The concept of co-administration of an anticancer drug with an ABCG2 inhibitor is attractive, because the improved bioavailability of anticancer drugs allows oral dosing, which is more practical than parenteral application of a drug. Preclinical and clinical research shows that inhibition of ABCG2 effectively increases the oral bioavailability of various anticancer drugs (72-75). However, taking into consideration the housekeeping role of ABCG2 in many cell types, there is a great potential for unexpected organ toxicity regarding the application of these emerging chemotherapeutic agents specifically targeting ABCG2.

Table 2. Inhibitors of ABCG2 (Generated from data, published in references (36,51,70,71))

Dietary inhibitors	Apigenin, Biochanin A, Chrysin, Curcumin, Flavonoids, Folate, Genistein, Hesperetin, Kaempferol, Naringenin, Pyridines derivatives, Silymarin, Xanthine
Exogenous inhibitors	Chromanone derivatives, Cyclosporin A, Elacridar, Erlotinib, Flavopiridol, FTC, Gefitinib, Imatinib, KO132, KO134, KO143, KS176, Lapatinib, Nilotinib, Novobiocin, Pantoprazole, Pipecolinate derivatives, PSC0833, PZ39, Reserpine, Sunitinib, TAG11, TAG139, Tamoxifen, Tariquidar, Taxane derivatives, Toremifene

ABCG2 in the heart

Although the heart has long been considered as an organ without regenerative capacity, it has become evident that resident multipotent stem cells are in continuous action -differentiating into endothelial cells, smooth muscle cells or myocytes if needed-, in order to maintain cardiac function (76). Just like in the stem cells of other organs, ABCG2 is present in cardiac stem cells, where it modulates the progression of cardiac progenitor cell cycle and asymmetric cell division (77). Besides progenitor cells, ABCG2 is expressed mainly in endothelial cells of cardiac capillary vessels, and it is present in the plasma membrane of cardiomyocytes (78,79). In microvascular endothelial cells, ABCG2 regulates the transport of glutathione, -an important endogenous antioxidant- and by promoting angiogenesis and antioxidant response, it protects against pressure overload-induced cardiac hypertrophy and heart failure (80). It has been shown that after myocardial infarction, ABCG2 plays a crucial role in cardiac repair through the modulation of microvascular endothelial cell function (81). ABCG2 was also shown to be highly upregulated in end-stage heart failure in man (79).

Diastolic Dysfunction - Cardiac Fibrosis

The cardiac cycle is basically built up of systole and diastole. Systolic function reflects the contraction of the ventricle causing ejection, while diastolic function implies its relaxation causing filling of the ventricles. Diastole is the period during which the ventricular chambers of the heart stop generating force, return to an uncontracted state and get filled with blood. Diastolic dysfunction therefore refers to the impairment of ventricular relaxation, -filling or -distensibility, when the myofibrils do not rapidly or completely return to their resting length, the ventricular chamber volume becomes slightly smaller and the filling pressure increases (82). The basic mechanisms that underlie diastolic dysfunction may be intrinsic due to altered calcium handling of the cardiomyocytes (83), or may be a consequence of abnormalities in the passive components (extracellular matrix) of the ventricle (84).

The active phase of relaxation is a series of energy-consuming steps starting with the calcium ion dissociating from troponin, followed by actin-myosin crosslink detachment, calcium reflux into the sarcoplasmic reticulum, sodium/calcium exchanger-mediated calcium efflux from

the cytoplasm, and extension of the sarcomere to its resting length (85). If the energy supply is sufficient and sustainable, these active cellular relaxation processes occur at proper rate and extent, therefore the ventricular relaxation happens in the proper rate and extent as well. This results in the decline of ventricular pressure at constant volume (isovolumic relaxation), then followed by chamber filling, when both volume and pressure parameters are dynamically changing (86). The passive viscoelastic properties of the ventricle are particularly crucial in this second phase of diastole, as they greatly influence the capability of the myocardium to return its resting force and length. This can also be seen in patients with diastolic heart failure, as they display abnormalities in passive stiffness of the ventricle which can be also described by the term - pulmonary artery wedge pressure (PAWP)/cardiac output (CO) as increased LV filling resistance (87,88). Impaired ventricular relaxation at end-diastole causes elevated end-diastolic pressure (EDP) which is a well-established indicator of diastolic heart failure and predictor of mortality (89). Structural changes of the myocardium – like collagen deposition (fibrosis) – results in increased passive myocardial stiffness and EDP elevation, therefore myocardial fibrosis is related to the severity of diastolic dysfunction (90,91)(92).

In the heart, the primary mechanical role of the extracellular matrix is to provide a supportive scaffold for the myocardium which prevents sarcomere-overstretching, myofibre slippage, sustains ventricular chamber geometry, and protects against rupture (93). In addition, it has a secondary functional role, influencing the electrical behaviour of the myocardium and the vascular reactivity of its coronary microvasculature (94). This extracellular scaffold co-ordinates the mechanical forces generated within myofibres, facilitating the physiological contraction of the ventricular chambers. On the other hand, the energy during each systolic contraction can be stored in this elastic myocardial scaffold, which is getting released in diastole, when extracellular matrix fibers return to their neutral shape, ultimately providing energy for diastolic suction (84).

The matrix-component deposition in adult hearts is normally very low, yet if it is perfectly aligned it greatly supports cardiac function. The adverse effects arise when collagen content increases dramatically in the myocardium, since passive tissue stiffness increases in response

to a massive deposition of stiff, heavily crosslinked collagen. The detrimental impact of this collagen accumulation on diastole has been shown in both humans and in experimental animal models (90,95-97).

The cells primarily responsible for myocardial collagen deposition are cardiac fibroblasts, representing the main cellular component of the heart -beside cardiomyocytes. These flat, spindle-shaped cells have mesenchymal origin and are the only cells in the heart lacking basement membrane (98,99). Cardiac fibroblasts are termed as sentinel cells, because they sense changes from the microenvironment and react to these in order to maintain structural integrity, and preserve organ function. Fibroblasts contribute to structural, mechanical, electrical and biochemical properties of the myocardium. They respond to stimuli in various ways, including proliferation and migration, or secretion of cytokines and growth factors. However, the primary function of the cardiac fibroblasts is the dynamic regulation of the synthesis and degradation of collagen and extracellular matrix (98). When cardiac fibroblast-mediated collagen synthesis exacerbates, it leads to pathological extracellular matrix deposition, increasing myocardial stiffness (99).

Aims

In the present study, we aimed to explore the role of ABCG2 in hypoxia-induced pulmonary hypertension and in the cardiac function under stress. Special attention was given to the structure and the function of the heart, as in pulmonary hypertension the main cause of mortality is right ventricular failure. In order to delineate the possible role of ABCG2, we employed the chronic hypoxic mouse model, as it provides the advantage to investigate the development of PH and the hypoxia-induced changes on myocardial function simultaneously.

Materials and Methods

Animals

Male ABCG2 knockout mice were obtained from Taconic Europe (Laven, Denmark) on FVB/N background. ABCG2 KO mice have been originally developed by two independent groups (54,100). Although these mice appear to lack any obvious phenotype under normal conditions, it was accidentally discovered that ABCG2 null mice fed on special diet containing alfalfa (*Medicago sativa*) leaf concentrate, develop skin lesions caused by pheophorbide-A, a phototoxic protoporphyrin catabolite of clorophyll (100).

In our experiments, we placed 10-12 week old mice (10 per group, wild type (WT) and KO) in normobaric hypoxic chambers [fraction of inspired oxygen (FiO_2) of 0.10] for 4 weeks to establish the chronic hypoxia-induced pulmonary hypertension model. Control animals were in normobaric normoxia (FiO_2 of 0.21) for 4 weeks. The oxygen concentration was monitored continuously and sustained using OxyCycler programmable gas controller system (BioSpherix, Lacona, NY, USA). All experimental mice were kept under conventional conditions on chow-fed diet. All experiments were approved by the local authorities according to national regulations (Austrian Ministry of Education, Science and Culture, BMWF-66.010/0062-II/3b/2012).

Haemodynamic measurements

Ventricular pressure measurements were obtained through cardiac catheterization under constant inhalation of 2% isoflurane-oxygen narcosis mixture, using the closed chest technique, as described previously (101). The insertion of the catheter into the right jugular vein made excess into the right ventricle, where pressures values were recorded. Afterwards, the catheter was placed into the right carotis to measure blood pressure, and then forwarded into the left ventricle in order to record pressure values from this ventricle as well. For data collection SPR-671 1.4F catheters (Millar Instruments Inc., Houston, USA) were used with a sampling rate of 1kHz, coupled to a Millar PCU-2000 pressure control unit

and PowerLab 8/30 acquisition system (AD Instruments, Spechbach, Germany). Prior to the operation, the catheter was placed into a fluid-filled tube in order to calibrate to atmospheric pressure (0.1 mmHg accuracy). The recordings were analysed using Powerlab Pro Software (AD Instruments, Spechbach, Germany). End-diastolic pressure (EDP), Tau index, mindP/dt or maxdP/dt were calculated with the software´s analysis feature. Haemodynamic measurements of the left ventricle were performed following data collection from the right ventricle, which itself is a laborious procedure. In certain animals, the haemodynamic system became unstable by the time of left ventricular measurements, therefore they were excluded from the analysis. As well, in some animals the quality of pressure recording was not adequate for measuring precise LVEDP or RVEDP (Tau, mindP/dt, maxdP/dt) by the applied analysis module of the software. (Text modified from (102)).

Assessment of right heart hypertrophy

After cardiac pressure measurements, the mice were sacrificed, lungs and hearts were perfused with PBS via the right ventricle. The atria was removed from the heart, the right ventricle (RV) was separated from the left ventricle + septum (LV+S) and these regions were measured in order to obtain the mass ratio of the right ventricle to the left ventricle plus septum (RV/(LV+S)) or to the body weight of the mouse (RV/BW).

Cytokine and chemokine measurements

Serum samples from hypoxia-treated WT and ABCG2 KO mice (n:4 WT and 4 KO) was profiling to investigate circulating cytokines, using a mouse cytokine array kit (#ARY006, R&D systems, Minneapolis, USA). The array was performed according to manufacturer´s protocol. Briefly, 50µl samples were mixed with the kit´s biotinylated antibody and incubated overnight (4°C) with the provided nitrocellulose membranes, where chemokine-specific antibodies were spotted as duplicates. During development, the obtained chemiluminescent signals were captured on X-ray films, and were analysed using ImageJ (Bethesda, Maryland,

USA). The signals – as pixels - were proportional to the amount of captured cytokines. Correspondent pixel densities are shown as arbitrary units normalized to the manufacturally included reference spots. (Text modified from (102)).

Pulmonary arterial banding

The pulmonary arterial banding (PAB) was performed as described previously (103). The experimental mice were primarily anesthetized (i.p. fentanyl 0.05 mg/kg and midazolam 5 mg/kg) and the narcosis was continued with 2-3% isoflurane-oxygen mixture, using mechanical ventilation supplied by a Minivent system (Hugosachs, March-Hugstetten, Germany). In sterile conditions the pericardium was removed through an incision in the left 2^{nd} intercostal space, than a partially occlusive titanium clip was inserted around the pulmonary artery (Weck, Research Triangle Park, NC, USA). With this the pulmonary artery became congested to 0.30 mm, corresponding to an approximately 75% occlusion of the vessel lumen. After the operation the incision was closed, and the mice were allowed to recover from anaesthesia. Post-operative analgesia was applied as a s.c. Buprenorphine (0.1 mg/kg) per day for 3-5 days depending on animal's condition. Sham-treated mice underwent identical surgical procedure but the banding clip was placed next to the pulmonary artery. (Text modified from (102)).

Mouse cardiac fibroblast isolation

Mouse cardiac fibroblasts were isolated using mechanical disruption and enzymatic digestion of the ventricular tissue. After 9 weeks old mice were exsanguinated, the hearts were removed and perfused with 1000µl digestion buffer (Krebs-Ringer solution, supplemented with 1mg/ml BSA, 2.5mM CaCl2 and 0.5 mg/ml collagenase II), retrogradely from the aorta. The connective tissue, atria and vessels were removed from the heart. The right ventricle was disjointed, the left ventricle was cut open, and both were washed free of blood. 3 right- and 3 left ventricles were combined separately and minced into small pieces

in digestion buffer. Afterwards 3 repetition of digestion step was performed on 37°C for 6 minutes. In between, tissue pieces were pipetting up-and down, until no visible tissue fragments were present in the solution. The obtained cell suspensions were plated in tissue culture flasks (T75) in DMEM/F-12 medium((1:1) (Gibco by life technologies, Paisley, UK), supplemented with 10% FCS, 1% L-glutamine and 0.2% antibioticum-antimycoticum), and this culture medium was changed after 3 hours. Adherent cells were cultivated till ~90% confluency, than detached using trypsin, and further cultured until passage 3 for experiments. The purity of the isolated ventricular fibroblasts was confirmed by the expression of characteristic fibroblast markers. (Text modified from (102)).

Mouse lung fibroblast isolation

Mouse lung fibroblasts were isolated using mechanical disruption of the lungs. After 9 weeks old mice were exsanguinated, the lungs were removed and cut free of trachea and bigger vessels. The lungs of 3 mice were combined, dissected into small pieces and passed through a 0.1mm mesh to exclude bronchi and vessels. The obtained cell suspensions were plated in tissue culture flasks (T75) in DMEM/F-12 medium((1:1) (Gibco by life technologies, Paisley, UK), supplemented with 10% FCS, 1% L-glutamine and 0.2% antibioticum-antimycoticum), and this culture medium was changed after 2 days. Adherent cells were cultivated till ~90% confluency, than detached using trypsin, and further cultured until passage 3 for experiments. The purity of the isolated lung fibroblasts was confirmed by the expression of characteristic fibroblast markers.

Human lung samples

Lungs were obtained from patients underwent lung transplantation at the Department of Surgery, Division of Thoracic Surgery, Medical University of Vienna, Austria. Non-implanted, non-tumorous donor lungs that had not been used for transplantation –due to size limitations- served as controls. All experiments on diseased and donor samples involved in

the current study were approved by the institutional ethics committee (976/2010) of Medical University of Vienna, and written consent was obtained before from all study participants. All lungs were extensively reviewed by experienced pneumologists and pathologists to confirm diagnosis at the time of transplantation.

During sample preparation, sagittal sections of the respective lungs were performed and cut free from pleura. The subpleural region was then sampled as $1cm^3$ peripheral tissue blocks, which were either snap-frozen for RNA analysis or transferred to 4% (m/v) paraformaldehyde for histochemical analyses.

Human pulmonary arterial smooth muscle cells (hPASMC)

Primary human PASMCs were isolated from the resistance pulmonary arteries of non-transplanted healthy donors. The purity of the cells was confirmed by immunohistochemistry using antibody against smooth muscle-specific isoforms of alfa-actin. VascuLife Complete SMC Medium (LifeLine Cell Technology, Frederick MD, USA) supplemented with 20% FCS (Lactan, Graz, Austria) and 1% antibiotics (LifeLine Technology) was used for culturing. For all experiments, PASMC underwent no more than one freeze/thaw cycle and cells were used no longer than the 6^{th} passage.

Human pulmonary arterial endothelial cells (hPAEC)

Human pulmonary artery endothelial cells (hPAECs) were purchased from Lonza (Allendale, New Jersey, USA) and were cultured in Vasculife-endothelial specific media (LifeLine Cell Technology, Frederick MD, USA) according to the manufacturer's instructions. Cells in passages 5–9 were used for the experiments.

Human Cardiac fibroblasts (hCFs)

Cardiac fibroblasts isolated from human ventricles were purchased from Promocell, and were grown in complete fibroblast medium (Fibro Life® S2). Cells in passages 2-7 were used for the experiments.

Cell culture and stimulation

Prior to all stimulations, cells were kept overnight in starvation medium (VascuLife® Basal Medium 0%FCS supplemented with 1% P/S), and maintained in basal medium during the experiment, in case of hPASMCs and hCFs. Starvation, and treatments for mouse CFs were performed in DMEM/F12 (1:1) medium containing 2% FCS and 0.2% P/S, whereas hPAEC starvation plus treatments were carried out in VascuLife® Basal Medium with 2% FCS and 1% P/S. Both cell types were maintained in incubators (Binder, Tuttlingen, Germany) at 37°C with 5% CO2. Hypoxic cell culturing and treatment were carried out in a hypoxic work station (BioSpherix, Lacona, NY, USA) including fully-integrated hypoxia incubators, supplied with programmable oxygen control and non-condensing humidity control at 37°C. Hypoxia (FiO2 of 0.01) was used for 48 hours.

Silencing of cardiac fibroblasts

Small interfering RNA directed against ABCG2 was purchased from Santa Cruz Biotechnology (#sc-41151 (human), #sc-37054 (mouse), Santa Cruz Biotechnology, Heidelberg, Germany). A non-silencing, commercially available negative-control siRNA was employed for control experiments (#sc-37007, Santa Cruz Biotechnology, Heidelberg, Germany). The transfections were carried out using Amaxa Basic Nucleofector Kit (#VPI-1002, Lonza, Cologne, Germany). The down-regulation of the targeted protein was assessed after 48 hours by qPCR and after 72 hours by western blotting.

Proliferation assay

Cardiac fibroblasts were silenced as it is described in "Silencing of cardiac fibroblasts"-section, and were plated in 96 well plates as 20.000 cells/well. The following day, the cells were treated with preincubated (12h) hypoxic VascuLife® Basal Medium (2% FCS, 1% P/S), and were placed in hypoxia (FiO_2 of 0.01). After 24 hours, [3H]-thymidine (2μCurie/ml, American Radiolabeled Chemicals, St.Louis, USA) was administered for an other 24 hours, when thymidine incorporation was measured as an index of DNA synthesis - proliferation rate-, using radioactive scintillation counter (Wallac 1450 MicroBeta TriLux, Minnesota, USA). Experiments were carried out in quintuplicates.

Immunohistochemistry

Mouse hearts were dissected for determining right ventricular hypertrophy, then fixed in 4% formalin and processed into paraffin for sectioning. Lungs were perfusion-fixed through the trachea (with 4% formalin), and embedded into paraffin as well. These formalin-fixed paraffin-embedded heart and lung blocks were cut to 3,5 μm thick sections and stained with Masson's trichrome to determine collagen content. The percentage of fibrosis in right ventricles, in left ventricles + septum and in the lungs was quantified on the whole specimen area using semi-quantitative image analysis software (Visiopharm, Hoersholm, Denmark). Antigen retrieval was performed with 0,01M sodium citrate solution (pH 6.0) in 95^{o}C. ABCG2 expression was visualized using ABCG2 antibody (#AV43649, Sigma-Aldrich, Saint Louis, USA). Assessment of capillary density in the right heart and in left ventricle + septum was carried out using thrombomodulin (#AF3894, R&D systems, Minneapolis, USA) staining. The capillary density was quantified using semi-quantitative image analysis software (Visiopharm, Hoersholm, Denmark) and reported relative to the total sample area. As negative controls, duplicates were processed without primary antibodies. Slides were digitised using slide scanner (Aperio, Oxford, UK) using 40x magnification objective. (Text modified from (102)).

Masson`s trichrome staining

The slides were deparaffinised and re-fixed using Bouin's solution (25% formaldehyde (37-40%), 75% saturated picric acid, 5% glacial acetic acid) followed by rinsing with running tap water for 5-10 minutes. Then nuclei were stained with Weigert`s iron-hematoxylin solution (1:1 mixture of 1% hematoxylin in 95% EtOH and 4% FeCl (29%), 1% HCl in dH2O) for 10 minutes, rinsed and incubated in Biebrich scarlet acid fuchsin (90% Biebrich scarlet (1% acqueous), 9% Acid fuchsin (1% acqueous) and 1% glacial acetic acid) for 10 to 15 minutes in order to stain acidophilic structures such as collagen and cytoplasm red. After rinsing, a 10 to 15 minutes of phosphomolybdic-phosphotungstic acid solution (1:1 ratio of 5% PM acid and 5% of PT acid) incubation removed the red colour of the collagen. Then the collagen was stained blue with Aniline blue solution (2.5% Aniline blue, 2% glacial acetic acid in dH2O). At last the staining was differentiated using 1% acetic solution for 3 minutes. Afterwards the slides were dehydrated using increasing percentage of EtOH and mounted with xylol-based mounting media (Thermo Scientific). (Text modified from (102)).

Immunofluorescence of tissues

Tissue sections were deparaffinised at 60°C for 2h, and incubated with trypsin at 37°C for 20min. After a blocking step with 10% BSA/PBS (40 min), the slides were incubated at 4°C overnight with ABCG2- (#AV43649, Sigma-Aldrich, 1:100 in 10% BSA/PBS) or Vimentin (Abcam #ab11256, 1:200 in 10% BSA/PBS) antibodies, and detected with Alexa Fluor 555 and 488 secondary antibodies (Life Technologies, 1:500 in 0.1% BSA/PBS) at room temperature for 45min. Counterstaining of nuclear DNA was performed with 4´,6-diamidino-2-phenylindole dihydrochloride (DAPI) (Sigma-Aldrich). As negative control, duplicates were processed without primary antibodies.

Immunofluorescence of cells

Fibroblasts were fixed with 4% paraformaldehyde and incubated at 37°C for 20 min. Afterwards the cells were rinsed with PBS (3X) and permeabilized with 0.1% Triton-X100/PBS

at room temperature for 15 min, followed by a blocking step with 3% BSA/PBS at room temperature for 30 min. Then cells were incubated at 4°C overnight with ABCG2- (#ab3379, Abcam, 1:100 in PBS), S100A4- (#ab27957, Abcam, 1:200 in 0.1% BSA/PBS), Periostin- (#ab14041, Abcam, 1:200 in 0.1% BSA/PBS), Fibronectin- (#ab23750, Abcam, 1:100 in 0.1% BSA/PBS) or Vimentin- (#ab11256, Abcam, 1:400 in 0.1% BSA/PBS) antibodies respectively. Afterwards, Alexa Fluor 555-labelled secondary antibody (Life Technologies, 1:1000 in PBS, except F-actin) was applied at room temperature for 30 min at. Counterstaining of nuclear DNA was performed with 4´,6-diamidino-2-phenylindole dihydrochloride (DAPI) (Sigma-Aldrich). As negative control, duplicates were processed without primary antibodies. Pictures were taken with Olympus Basic BX61VS Fluorescence microscope at 40X magnification.

Hydroxyproline assay

Mouse or human fibroblasts were plated in 6 well plates as 200.000 cells/well, after gene silencing. After 24 hours the media was changed to VascuLife® Basal Medium (2% FCS, 1% P/S for human cells) or DMEM/F-12 (1:1) (2%FCS with 0.2% P/S for mouse fibroblasts) hypoxic (FiO2 of 0.01) medium, and plates were immediately placed into hypoxia (FiO2 of 0.01) for 48 hours. Then protein samples of the cells were collected, and were hydrolysed using 6M HCl (95°C for 20 hrs). After cooling down the samples to room temperature, they were centrifuged (13,000 x g, 10min), and supernatants were incubated (60°C, 2 hours) with detection reagents provided by the manufacturer (Quickzyme Biosciences, Leiden, The Netherlands). The absorbance was then detected using spectrophotometer at 570nm. (Text modified from (102)).

Western blot analysis

Protein extracts of the cells and tissues were collected using radioimmunoprecipitation assay (RIPA) buffer containing inhibitors of proteases and phosphatases (Roche, Vienna,

Austria). Equal amounts of protein were then separated on sodium dodecyl sulfate (SDS) polyacrylamide gels, followed by electro-transfer to nitrocellulose membranes. In order to avoid nonspecific binding of antibodies, the membranes were blocked by 5% (m/v in TBS-T(20 mM Tris-Cl, pH 7.5, 150 mMNaCl, 0.1% (v/v) Tween 20)) non-fat dry milk at room temperature for 60 min. Then, samples were incubated overnight at 4°C with antibodies listed in *Table 5*. The next day, the membranes were incubated in room temperature for 1 hour with peroxidase-labelled secondary antibody (Pierce Biotechnology, Rockford, USA), and the signals were detected using West Pico Substrate (Thermo Scientific, Rockford, USA) or Enhanced ChemiLuminescence kit (Amersham Biosciences, Buckinghamshire, UK).

RNA extraction and Q-PCR Analysis

From formalin-fixed paraffin-embedded mouse ventricles, RNA was extracted using QIAGEN RNeasy FFPE Kit (#73504, Qiagen, Hilden, Germany). From cells RNA was obtained by peqGOLD RNA isolation kit (PeqLab, Erlangen, Germany). In order to quantify the purity and the concentration of isolated total RNA, Nanodrop 2000c spectrophotometer (Nanodrop, Rockland, USA) was used. Isolated RNA was reverse transcribed by using iScript cDNA Synthesis Kit (BioRad, CA, USA) according to the following protocol steps: 5 min at 25°C, 30 min at 42°C, 5min at 85°C. The products were either used directly for quantitative real time PCR (qRT PCR) or stored at -20°C. Gene expression was measured by qRT PCR using QuantiFast SYBR Green Kit (Qiagen, Hilden, Germany). Reaction mixtures contained SYBR Green mastermix, forward and reverse primers (*Table 3 and 4*), and cDNA samples. Amplification was quantified in duplicates by Lightcycler 480 system (Roche) according to the following protocol: 1× (95°C, 5 min); 40× (95°C, 10s; 60°C, 30s). The data for amplification curves were acquired after the extension phase at 60°C. In order to validate PCR products, melting curves were analysed after amplification. The expression of targeted genes are presented as ΔCT normalized to the level of Beta-2 microglobulin (B2mg) housekeeping gene, using the following formula ΔCT = CT(Housekeeping Gene) – CT(Gene of Interest).

Statistical analysis

Values are given as means ± SD for all measurements, except if stated otherwise. Statistical analysis was performed with GraphPad Prism 5 and SPSS Statistics software (IBM, USA: SPSS Inc., Institute for Medical Informatics, Statistics and Documentation, Medical University of Graz). For comparison of two groups, Mann-Whitney U test was carried out (p values <0.05 were considered significant).Differences according to the genotype (KO vs. WT) and the treatment (normoxia vs. hypoxia) and their interactions were analysed by adjusted rank transformed two-way ANOVA. For post hoc analysis of the interaction, KO and WT mice were compared separately in both treatment (normoxia vs. hypoxia), and normoxia vs. hypoxia were compared separately within both genotypes using Bonferroni adjusted Mann-Whitney U Test (four comparisons). Due to the exploratory character of the study, no p-value adjustment was applied for the analysis of main effects and interactions in the different parameters. The effects of hypoxia and genotype are presented in the adjusted rank transformed two-way ANOVA *Table 6*. (Text modified from (102)).

Tables

Table 3: Human primers

Gene name	Access. No.	Forward primer (5′- 3′)	Reverse primer (5′- 3′)	Ampl. size
ABCA1	NM_005502	GCACTGAGGAAGATGCTGAAA	AGTTCCTGGAAGGTCTTGTTCAC	204
ABCA2	NM_001606	CATCCCCCTGGTGCTGTTCTT	GCTTGGGCCGTGCTATTGG	446
ABCA3	NM_001089	GCCCTCTTTACACTCAGTTTTCA	GACGAGCAGTTGTCGTACCTAAT	502
ABCA4	NM_000350	TGGTCAAAGCCTGGGAAGAAGTA	TCCAGGGATACATGTCAGGGAAT	404
ABCA5	NM_018672	GGGCCCAATGGTAGGAGGTAGAG	TGAGGAATGGGCAAGGGAGGT	255
ABCA6	NM_080284	CCGTCAAGGGGCTCAGGAA	GATGGCCACACGGTCACAC	316
ABCA7	NM_019112	CCCGGCCACGTGCGCATCAAAAT	CCACCGCGAAGGCTGCCAAGAACA	537
ABCA8	NM_007168	AGTGCGCGGGCTCTTCTTTGT	GTTTTCCTTCGCTTTTGGCTGATA	155
ABCA9	NM_080283	CCCCATGATGAAAGAGCACAGAG	AGGATCCCCCAAAAGACAATAAGG	596
ABCA10	NM_080282	ATGGCTCAGATGATCCCTCCTACA	CTCCGTTTGAATAAGCTCCGTGAA	175
ABCA12	XM_049831	TCTCGCCGAAGTATATGGGATGTT	GGCTTCGGGGAGATGTGATTG	281
ABCB1	NM_000927	TGACATTTATTCAAAGTTAAAAGCA	TAGACACTTTATGCAAACATTTCAA	307
ABCB2	NM_000593	AGGGCTGGCTGGCTGCTTTGA	ACGTGGCCCATGGTGTTGTTAT	498
ABCB3	NM_000544	ACGGCTGAGCTCGGATACCAC	CCTCGGCCCCAAAACTGC	292
ABCB4	NM_018850	ACCGACTGTCTACGGTCCGAA	TCCATCGGTTTCCACATCAAGG	295
ABCB5	U66692	TCTGGCCCCTCAAACCTCACC	TTTCATACCGCCACTGCCAACTC	133
ABCB6	NM_005689	CAACCGCACCACCATCGTAGT	AATAAGCCAGGGAAAGGAGACACA	281
ABCB7	NM_004299	TGGGTCAGGGAAAAGCACAATAG	GGGGGTCCTTCAAAATGGCTCTT	361
ABCB8	NM_007188	GGGCCCACTGCATTGTCGT	CGGCCCCGGCTTTATTGT	333
ABCB9	NM_019625	GAGGGCCGGGTGGACTTTGAGAAT	CAGTGGGCAGGCCGTAGGAGATGT	378
ABCB10	NM_012089	ATGGGCGATATCTACGGAAACTGA	GGCGAGCTGGATAGGCAAAAT	518
ABCB11	NM_003742	AGGGAAATCAAGCTCTTAATGAAG	ATAGGTAGACTTATGATCTACAACA	187
ABCC1	NM_004996	AGTGGAACCCCTCTCTGTTTAAG	CCTGATACGTCTTGGTCTTCATC	551
ABCC2	NM_000392	TCCTTGCGCAGCTGGATTACAT	TCGCTGAAGTGAGAGTAGATTG	202
ABCC3	NM_020038	CAGAGAAGGTGCAGGTGACA	CTAAAGCAGCATAGACGCCC	269
ABCC4	NM_005845	TGATGAGCCGTATGTTTTGC	CTTCGGAACGGACTTGACAT	244
ABCC5	NM_005688	AGGGGCAAGAAAGAGAAGGTGAGG	GAGGGGGTCGTCCAGGATGTAGAT	566
ABCC6	NM_001171	GGCCCGGGCATCCAGGTT	TTTCATCTACGCGAGCATTGTTCT	430
ABCC7	NM_000492	CATTTTTGGCCTTCATCACATT	TGCCTTCCGAGTCAGTTTCAG	474
ABCC8	NM_000352	CTGCTAAACCGGATCATCCTAGCC	CGAGGAACACAGGTGTGACATAGG	195
ABCC9	NM_020298	GCTACAAAGTTGGCAGAGGC	TCCCAGGCATACAATTTTAGAAGT	136
ABCC10	U66684	GGCTCCGGCAAGTCTTCCCTGTT	AGATAGCTCCGGCCCCCTTCACC	304
ABCC11	NM_033151	CCACGGCCCTGCACAACAAG	GGAATTGCCAAAAGCCACGAACA	535
ABCC12	NM_033226	CACCGCCTCTATGGACTCC	TCAATCTCAGGCACTGGGGT	545
ABCD1	NM_000033	ACCAGGTGATCTACCCGGACTCAG	CTCACGGCGCTGGTGCATTCATCC	243
ABCD2	NM_005164	ATGGCCTGATTCGACCTCTCC	GTCTGCAGCGTTTCTCTTCCACT	294
ABCD3	NM_002858	CTCGGCCTGCACGGTAAGAA	TGGCAGCGATGAAGTTGAGTAAGT	300
ABCD4	NM_005050	GGATCTGAGCCTAAAGATCTCCGAG	GGGTCCCGTCAGTGAAGAATGGC	193
ABCE1	NM_002940	GGTTGCCTATCCCTCGTCCAG	TGTCCCCTTTGCCAGCCTTAG	262
ABCF1	NM_001090	ACAGGCTGGGGAAGAAGAGAAAGT	CAGGGCTGCAAAAACATTACCAC	255
ABCF2	NM_005692	TAGGGCGTTACCATCAGCATTTAC	GACCAGCATCATACCACCCTCAA	322
ABCF3	U66685	GGGGCATCAGACACGCTCAC	GTTGGGGCAGGGCATAGTCAT	256
ABCG1	NM_004915	CAGGAAGATTAGACACTGTGG	GAAAGGGGAATGGAGAGAAGA	176
ABCG2	NM_004827	CCGCGACAGTTTCCAATGACCT	GCCGAAGAGCTGCTGAGAACTGTA	380
ABCG4	NM_022169	GGTCTGGATAGCGCCTCTTGTTTC	ATGGGGCAGGGACCTCGTTCTTC	363
ABCG5	NM_022436	GCCGACTGTGCATGACTGCTCTG	TTACATTCTTGGGTCCGCTCAG	221
ABCG8	NM_022437	CCGGGGGCTTCATGATAAACTT	CTGAGGCCAATGACGATGAGGTA	234
β2mg	NM_004048.2	CCTGGAGGCTATCCAGCGTACTCC	TGTCGGATGGATGAAACCCAGACA	112

Table 4: Mouse primers

Gene name	Access. No.	Forward primer (5´- 3´)	Reverse primer (5´- 3´)	Ampl.
ABCG1	NM_009593.2	GCGCAGCCTCGTTCCTGCAA	GCTGGCATTCATGGCGGTGCC	131
ABCG2	NM_011920.3	GGCTTCACAGCTTTGCAGTAT	ACACAAGTGCTGTTGTCCGT	82
ABCG3	NM_030239.2	GCCGTAGGCACTGCTTTCCGT	GCAGGTAAAGTAGGCCAGCTCTCA	76
ABCG4	NM_138955.3	GGCAGGTGAAGAGAGCCGGA	CATCACGCAGCCGGCCTTGAC	138
ABCG5	NM_031884.1	AAGACCACGCTGCTGGACGC	ATCGCAACGTCTCGCGCACA	175
ABCG8	NM_026180.3	CCCAGCGTGACAAACGGGTGG	CCCCGGACACCCCACGTACA	102
ABCB1	NM_011076.2	AAATCCAGCGGCAGAACAGC	TGCCAAATGTGAAGCCCTGA	112
ABCC4	NM_001163676.1	CATCAAGTCCAGGGAAAAGGTTG	GAGGGCCGAGATGAGGGAG	72
Collagen1A1	NM_007742.3	CCCTGGTCCCTCTGGAAATG	GGACCTTTGCCCCCTTCTTT	72
Collagen3A1	NM_009930.2	TGACTGTCCCACGTAAGCAC	GAGGGCCATAGCTGAACTGA	105
Fibronectin	NM_010233.1	ACTGGATGGGGTGGGAAT	GGAGTGGCACTGTCAACCTC	104
TIMP1	NM_001044384.1	GAGACACACCAGAGCAGATACC	CAGCTACAGGCCTTACTGGAA	102
β2mg	NM_009735.3	CGGCCTGTATGCTATCCAGAAAACC	TGTGAGGCGGGTGGAACTGTG	115

Table 5: Antibodies

Antibody	Source	Dilution	Company	Product Nr.
p-PDGF receptorB	Rabbit	1:1000	Cell Signaling	3124
PDGF receptorB	Rabbit	1:1000	Cell Signaling	3169
Akt	Rabbit	1:1000	Cell Signaling	9272
p-Erk	Rabbit	1:1000	Cell Signaling	9101
Erk	Rabbit	1:1000	Cell Signaling	9102
Cyclin D1	Rabbit	1:1000	Cell Signaling	2978
P27	Rabbit	1:100	Santa Cruz	Sc-528
P21	Rabbit	1:1000	Cell Signaling	2947
ABCG2	Rabbit	1:1000 (WB,IH)	Sigma Aldrich	AV43649
ABCG2	Mouse	1:100 (IF)	Abcam	ab3379
ABCG2	Mouse	1:1000 (ventricles)	Abcam	ab3380
Thrombomodulin	Goat	1:100 (IH)	R&D	AF3894
GAPDH	Rabbit	1:2000	Santa Cruz	Sc-25778
α tubulin	Rabbit	1:2000	Cell Signaling	2425
α tubulin	Rabbit	1:1000	Abcam	ab4074
Vimentin	Goat	1:200 (IF)	Abcam	ab11256
S100A4	Rabbit	1:200 (IF)	Abcam	ab27957
Fibronectin	Rabbit	1:100 (IF)	Abcam	ab23750
Periostin	Rabbit	1:200 (IF)	Abcam	ab14041

Table 6: Adjusted rank transformed two-way ANOVA

Pulmonary hypertension - related parameters			
	Figure	Parameter	Significance
Interaction	Fig. 11	RVSP	p = 0.424
Genotype			p = 0.553
Hypoxia			p < 0.001
n numbers:	WT/nox:9, WT/HOX:9, KO/nox:10, KO/HOX:11		
Interaction	Fig. 10	LVSP	p = 0.759
Genotype			p = 0.501
Hypoxia			p = 0.037
n numbers:	WT/nox:8, WT/HOX:8, KO/nox:5, KO/HOX:7		
Interaction	Fig. 10	SBP	p = 0.609
Genotype			p = 0.712
Hypoxia			p = 0.064
n numbers:	WT/nox:9, WT/HOX:9, KO/nox:5, KO/HOX:11		
Interaction	Fig. 11	RV/LV+S	p = 0.419
Genotype			p = 0.094
Hypoxia			p < 0.001
n numbers:	WT/nox:9, WT/HOX:10, KO/nox:11, KO/HOX:11		
Interaction	Fig. 11	RW/BW	p = 0.411
Genotype			p = 0.265
Hypoxia			p < 0.001
n numbers:	WT/nox:9, WT/HOX:10, KO/nox:11, KO/HOX:11		
Interaction	Fig. 10	Hct	p = 0.705
Genotype			p = 0.694
Hypoxia			p < 0.001
n numbers:	WT/nox:7, WT/HOX:7, KO/nox:7, KO/HOX:7		

Right ventricular hemodynamic parameters			
	Figure	Parameter	Significance
Interaction	Fig. 13	RVEDP	p < 0.001
Genotype			p = 0.088
Hypoxia			p < 0.001
n numbers:	WT/nox:7, WT/HOX:7, KO/nox:7, KO/HOX:7		
Interaction	Fig. 14	Tau index	p = 0.631
Genotype			p = 0.079
Hypoxia			p = 0.883
n numbers:	WT/nox:6, WT/HOX:7, KO/nox:7, KO/HOX:7		
Interaction	Fig. 14	mindP/dt	p = 0.444
Genotype			p = 0.541
Hypoxia			p < 0.001
n numbers:	WT/nox:7, WT/HOX:7, KO/nox:7, KO/HOX:7		
Interaction	Fig. 14	maxdP/dt	p = 0.944
Genotype			p = 0.588
Hypoxia			p = 0.003
n numbers:	WT/nox:7, WT/HOX:7, KO/nox:7, KO/HOX:7		

Capillary density			
Interaction	Fig. 21	RV Capillary density	p = 0.057
Genotype			p = 0.752
Hypoxia			p = 0.951
n numbers:	WT/nox:7, WT/HOX:7, KO/nox:7, KO/HOX:7		
Interaction	Fig. 21	LV Capillary density	p = 0.716
Genotype			p = 0.822
Hypoxia			p = 0.129
n numbers:	WT/nox:7, WT/HOX:7, KO/nox:7, KO/HOX:6		

Left ventricular hemodynamic parameters			
	Figure	Parameter	Significance
Interaction	Fig. 15	LVEDP	p = 0.110
Genotype			p = 0.974
Hypoxia			p = 0.001
n numbers:	WT/nox:5, WT/HOX:7, KO/nox:5, KO/HOX:6		
Interaction	Fig. 16	Tau index	p = 0.165
Genotype			p = 0.922
Hypoxia			p = 0.267
n numbers:	WT/nox:5, WT/HOX:7, KO/nox:5, KO/HOX:6		
Interaction	Fig. 16	mindP/dt	p = 0.716
Genotype			p = 0.471
Hypoxia			p = 0.013
n numbers:	WT/nox:5, WT/HOX:7, KO/nox:5, KO/HOX:6		
Interaction	Fig. 16	maxdP/dt	p = 0.807
Genotype			p = 0.753
Hypoxia			p = 0.084
n numbers:	WT/nox:5, WT/HOX:7, KO/nox:5, KO/HOX:6		

Tissue fibrosis			
	Figure	Parameter	Significance
Interaction	Fig. 17	RV Fibrosis score	p = 0.036
Genotype			p = 0.216
Hypoxia			p = 0.009
n numbers:	WT/nox:6, WT/HOX:7, KO/nox:7, KO/HOX:7		
Interaction	Fig. 18	LV Fibrosis score	p = 0.002
Genotype			p < 0.001
Hypoxia			p < 0.001
n numbers:	WT/nox:6, WT/HOX:7, KO/nox:7, KO/HOX:7		
Interaction	Fig. 20	Lung Fibrosis score	p = 0.847
Genotype			p = 0.106
Hypoxia			p = 0.698
n numbers:	WT/nox:9, WT/HOX:10, KO/nox:11, KO/HOX:11		

Human cardiacfibroblasts			
	Figure	Parameter	Significance
Interaction	Fig. 28	Proliferation	p = 0.926
Silencing			p = 0.780
Hypoxia			p = 0.780
n numbers:	n:4		
Interaction	Fig. 28	Collagen production	p = 0.040
Silencing			p = 0.008
Hypoxia			p = 0.118
n numbers:	n:5		

Results

Section I.

Expression of ABC transporters in human lung

As the first step, we investigated the expression profile of ABC transporters, belonging to the ABC -A, -B, -C and -G family, in human IPAH lungs in comparison to donor lung homogenates (*Figure 1*).

In ABC-A family, ABCA4, ABCA5, ABCA9 were particularly highly regulated compared to the donor lungs. Moreover, in ABC-B, and -C family ABCB5, ABCB7 along with ABCC1, ABCC2, ABCC8, ABCC11, ABCC12 showed upregulation. The main interest of our study was the ABC-G family, where almost all of the family members (except ABCG1) were highly upregulated compared to donor lungs.

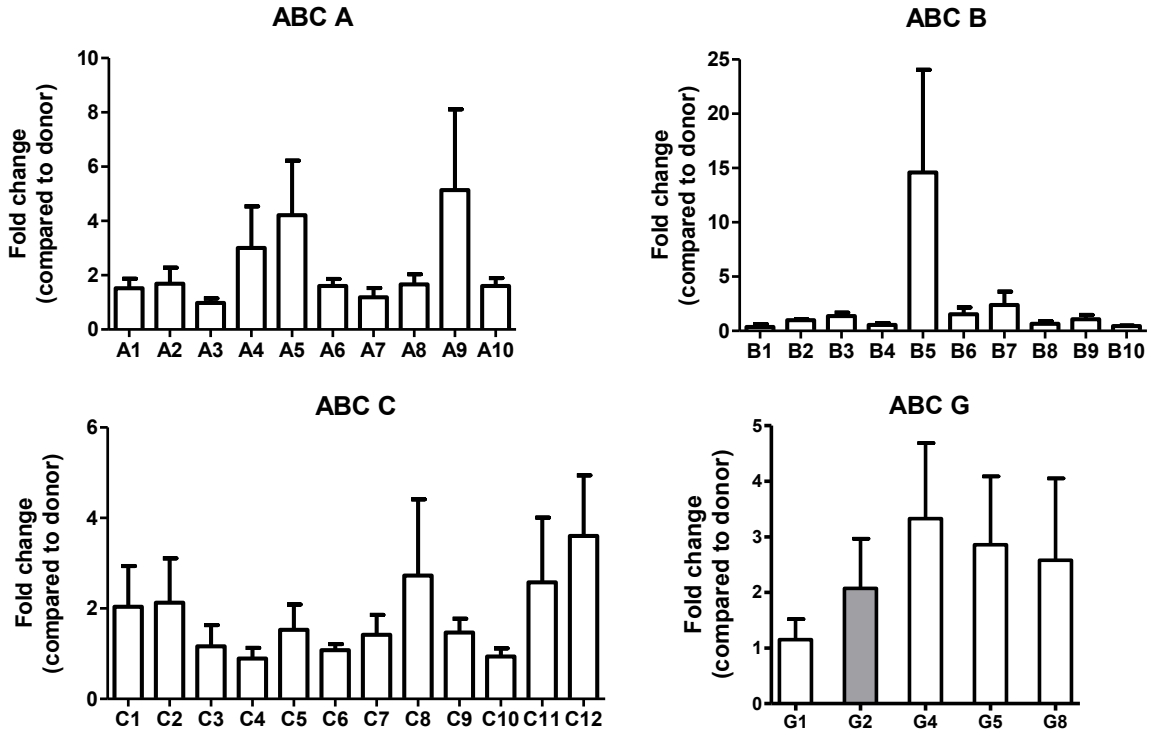

Figure 1: Expression of ABC transporters in human lung.

Relative mRNA expression from IPAH lungs compared to donor samples. Data presented in fold change. (donor n=6, IPAH n=7)

Since ABCG2 has been shown to provide protection from a variety of harmful agents (50), and to play a crucial role in survival under hypoxia (42), we were focusing on this particular transporter.

ABCG2 localization in human pulmonary vasculature

First, we assessed the preferential expression of ABCG family in human lung homogenate and hPASMCs and hPAECs. We found that ABCG2 mRNA was expressed in the human lung homogenates, hPASMCs and hPAECs (*Figure 2*). Further immunohistochemical staining against ABCG2 in donor and IPAH lungs revealed the strongest staining in the endothelial layer, moreover stainings were also observed in the smooth muscle layer of the vessels (*Figure 3*).

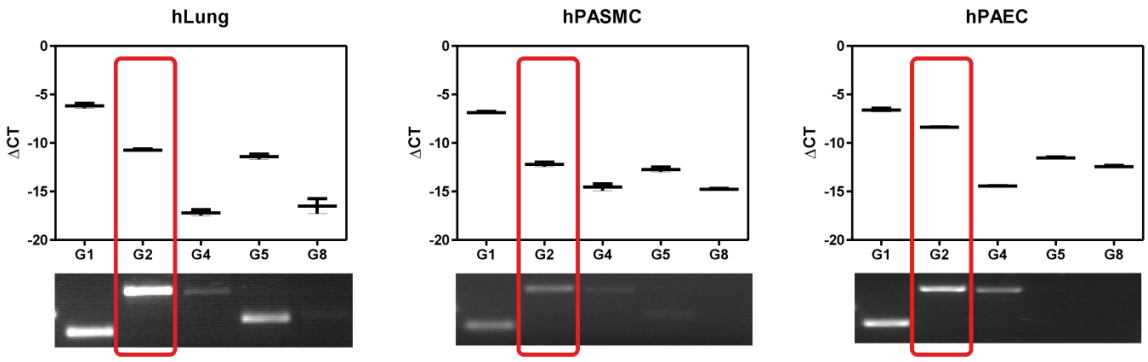

Figure 2: Presence of ABCG2 in the human lung.

Relative mRNA expression of ABC G family in donor human lung homogenates, hPASMCs and hPAECs quantified by qPCR (ΔCT=CT housekeeping gene- CT gene of interest) and RT-PCR followed by agarose gel electrophoresis (n=3).

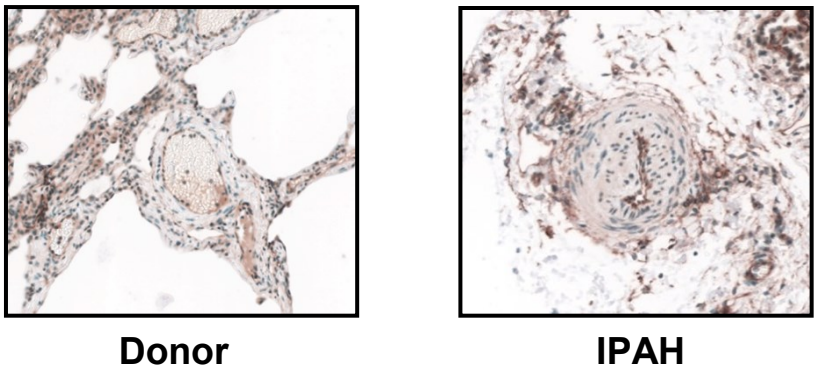

Figure 3: ABCG2 localization in human pulmonary vasculature.

Representative images of lung sections stained against ABCG2 from donor and IPAH patient.

PDGF induces ABCG2 expression in hPASMCs

As many other growth factors, platelet derived growth factor (PDGF) is extensively studied in human and animal models of pulmonary hypertension, where it was reported to play an important role in the pathogenesis of the disease (104). Moreover, it has been also shown that PDGF induces proliferation and migration of the cellular components of pulmonary arteries (105). Therefore in the next step, we investigated the PDGF-induced ABCG2 expression in hPASMCs. PDGF significantly up-regulated ABCG2 mRNA level in hPASMCs in a time dependent manner, attaining maximal regulation within 2-24 hours (*Figure 4*).

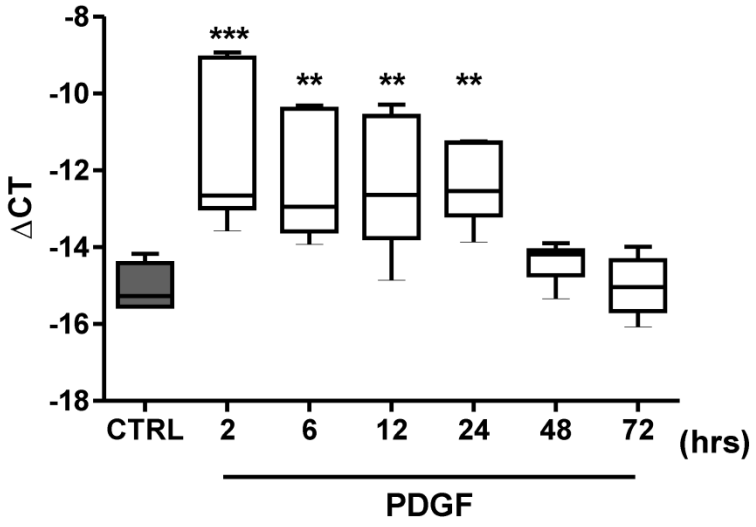

Figure 4: PDGF induces ABCG2 expression in hPASMCs.

Relative mRNA expression of ABCG2 with or without PDGF (10ng/ml) stimulation in hPASMCs were quantified by qPCR (ΔCT=CT housekeeping gene- CT gene of interest, *P<0.05).

Inhibition of ABCG2 suppresses PDGF induced proliferation

In order to investigate ABCG2 function on PASMCs, we utilized specific ABCG2 blockers (KS176 and KO143 (71,106)) to suppress its transporting abilities and thus, its role on cell proliferation. Blocking of ABCG2 with KS176 and KO143 showed a significant and dose dependent inhibition in proliferation of hPASMCs (*Figure 5), i*nduced by PDGF. 10µM of KS176 and KO143 showed the maximum inhibitory effect in the PDGF-induced proliferation in both cell types.

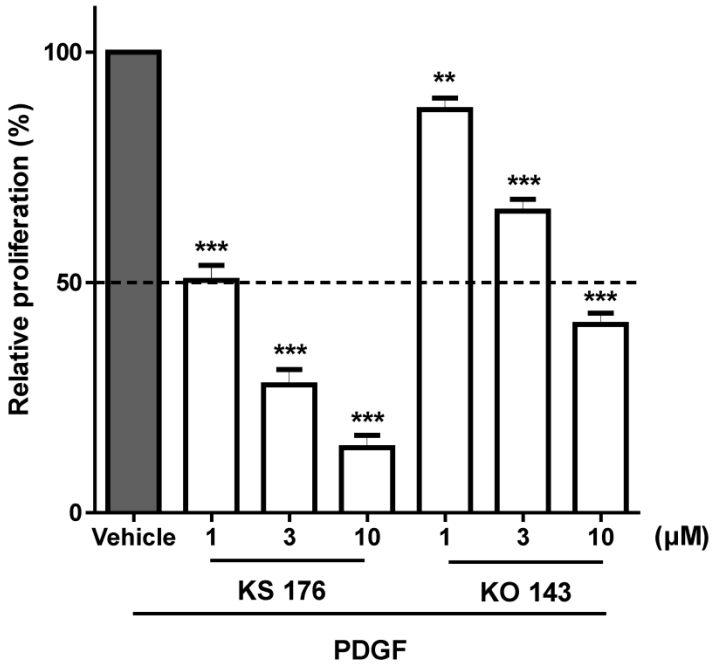

Figure 5: Inhibition of ABCG2 suppresses PDGF induced proliferation.

Proliferation assessed by relative 3H-thymidine incorporation in hPASMCs treated with KS176 or KO143 specific inhibitors of ABCG2 under stimulation of PDGF (10ng/ml, 48h).

To explain the observed inhibitory effect on PDGF-induced proliferation, next we investigated the effects of the inhibitors on the expression of known cell cycle-regulating proteins, such as Cyclin D1, p27 or p21 in PDGF-treated hPASMCs (*Figure 6*).

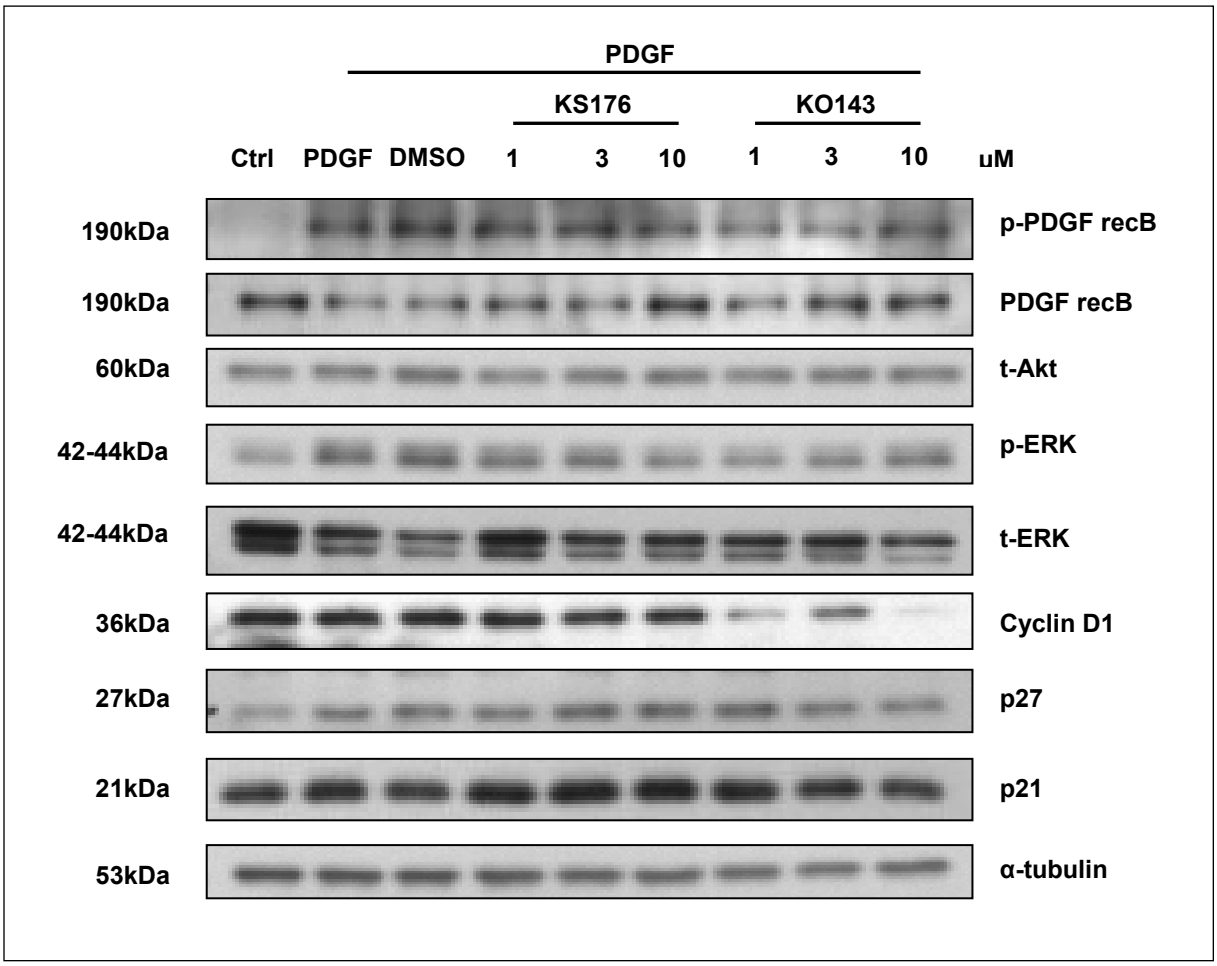

Figure 6: ABCG2 inhibition changes cell cycle-regulating protein expression in hPASMCs.
Western Blot analysis for phosphor-PDGFrecβ, PDGFrecβ, t-Akt, p-Erk, t-Erk, Cyclin D1, t-p27 ,t-p21 in hPASMCs treated with PDGF (10ng/ml, 48h) and different concentrations of ABCG2 blockers. α-tubulin is shown as loading control.

As expected, PDGF treatment resulted in the phosphorylation of PDGF receptor, as well it caused the phosphorylation of extracellular signal regulated kinase (ERK).

KO143 blocker reduced the amount of Cyclin D1 in PASMCs, but did not influence other investigated proteins. Cyclin D1 is a critical cell cycle regulator (107), therefore downregulation of it by KO143 could explain cell cycle arrest and a hampered proliferation observed before. On the other hand, KS176 did not have any effect on these cell cycle-related proteins, which leaves the question open, if the antiproliferative properties of this inhibitor is mediated by the investigated cell cycle proteins.

Section II.

To investigate the role of ABCG2 directly on an *in vivo* pulmonary hypertension model, we applied the animal model of the disease. Chronic exposure of hypoxia induces PH in mice, recapitulating most pathological alterations of the human condition, including pulmonary arterial contraction and remodeling, increased pulmonary arterial pressure and right ventricular hypertrophy (108).

First, we raised the question if ABCG2 has an altered regulation under hypoxia. Therefore we checked ABCG2 mRNA level in lung homogenates of wild-type mice, exposed to 10% hypoxia for 4 weeks. The quantification revealed a significant increase in ABCG2 expression in hypoxic mice compared to the respective normoxic controls (*Figure 7*).

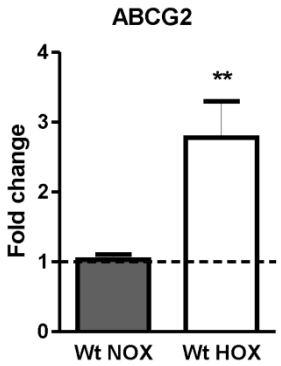

Figure 7: Expression of ABCG2 transporter in mouse lung after hypoxia.
Relative mRNA expression in lung homogenates of mice exposed to 4wks of hypoxia (10%) compared to normoxic (21%) controls. Data presented in fold change. (n=10 animals per group, mean ± SEM). (**p<0,01).

This upregulation of ABCG2 in mouse lung homogenate indicated, that ABCG2 might play important role in the lung, under hypoxic conditions. To investigate whether ABCG2 transporter has any effect in the development of PH in a murine model, we exposed wild-type and ABCG2 knockout mice to 10% hypoxia and normoxia and for 4 weeks.

ABCG2 knockout has no effect on hypoxia-induced pulmonary hypertension

In normoxia, we did not observe any differences between the two genotypes (wild type and ABCG2 knockout) in regards to heart rate, systemic blood pressure, left ventricular systolic blood pressure or blood haematocrit level (*Figure 8*). Similarly, right ventricular systolic pressure and right ventricular hypertrophy [Fulton index (RV/(LV +S))] was identical (*Figure 9*) in KO and wild type mice. However, in response to chronic hypoxia, blood hematocrit level, RVSP and Fulton index showed massive elevation independently of the genotype, showing that the lack of ABCG2 did not have an effect on the development of hypoxia-induced pulmonary hypertension.

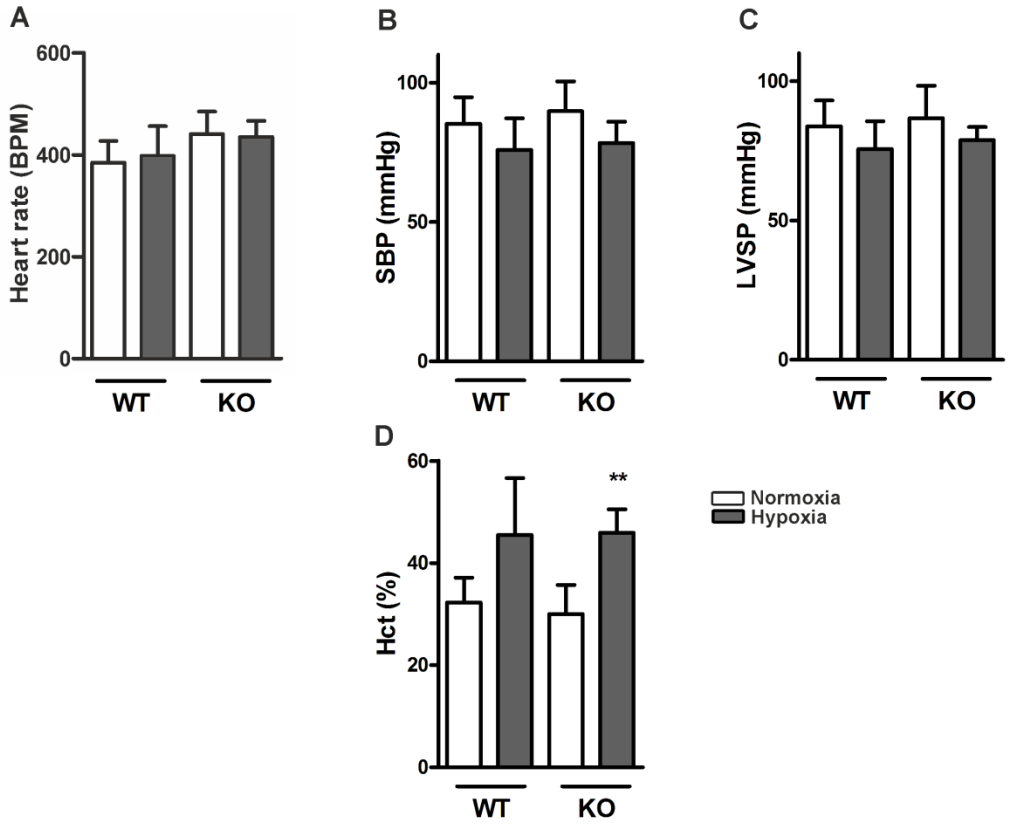

Figure 8. Hemodynamic measurements of chronic hypoxia treated mice

Bar graphs summarise (A) Heart rate in beats/minute (n= WT nox:9, WT HOX:9, KO nox:10, KO HOX:11), (B) systemic blood pressure (SBP) (n= WT nox:9, WT HOX:9, KO nox:5, KO HOX:11), (C) left ventricular systolic pressure (LVSP) (n= WT nox:8, WT HOX:8, KO nox:5, KO HOX:7) and percentage of blood haematocrit (Hct) levels in mice after normoxia or chronic hypoxia. Bar graphs represent values as means ±SD (* corresponds to hypoxic treatment within genotype; **p <0.01). Figure modified from (102).

We were also interested in, if these two factors – (I) hypoxic treatment and (II) the lack of ABCG2 – have any additive effect (interaction) on the readouts when concurrently present. Therefore, we have performed additional statistical analysis to test the presence of interaction. There were no interactions of hypoxia and genotype in any of the investigated parameters (*Figure 8 and 9*). (Text modified from (102)).

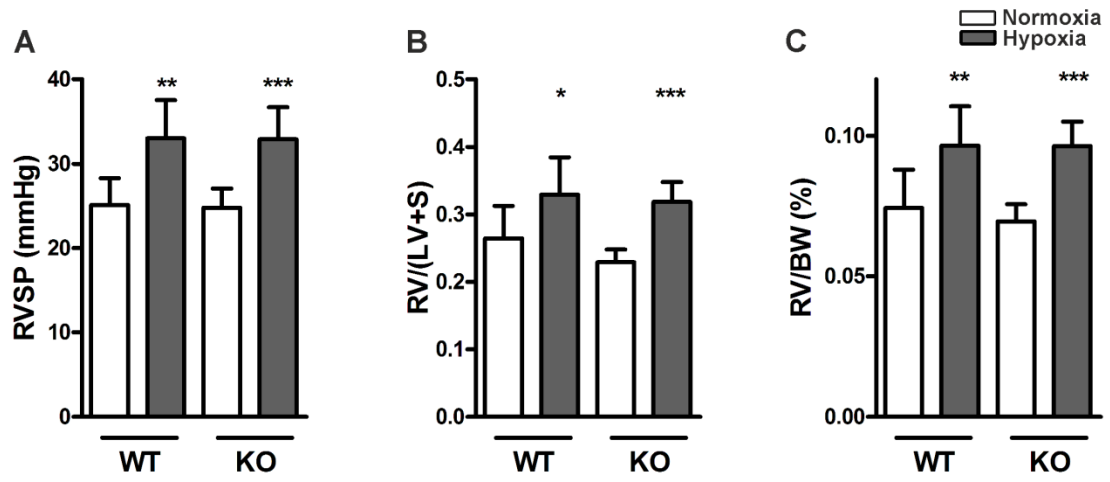

Figure 9. ABCG2 KO mice develop hypoxia-induced pulmonary hypertension

Bar graphs summarise (A) right ventricular systolic pressure (RVSP) (n= WT nox:9, WT HOX:9, KO nox:10, KO HOX:11), (B) right ventricular hypertrophy as right ventricular (RV) to left ventricular plus septum (LV+S) ratio) (n= WT nox:9, WT HOX:10, KO nox:11, KO HOX:11) and (C) RV to body weight (BW) ratio (n= WT nox:9, WT HOX:10, KO nox:11, KO HOX:11) of WT and ABCG2 KO mice exposed to normoxia or chronic hypoxia. Bar graphs represent values as means ±SD (* corresponds to hypoxic treatment within genotype; *p <0.05, **p <0.01, ***p <0.001). Figure modified from (102).

Taking our previous findings into account, one might expect that the development of PH is altered in the absence of ABCG2. As it was not the case, next we were investigating the gene expression of other, functionally related ABC transporters in the lung homogenate of the experimental mice (*Figure 10*). Out of the seven investigated ABC transporters, ABCB1 showed significant upregulation in ABCG2 KO mice under hypoxia. It has been shown previously, that ABCB1 and ABCG2 have a certain degree of substrate overlap (109), which allows to raise the hypothesis if the altered regulation of ABCB1 –or other ABC transporters as well- could have compensated the lack of ABCG2 in the lungs of hypoxic mice.

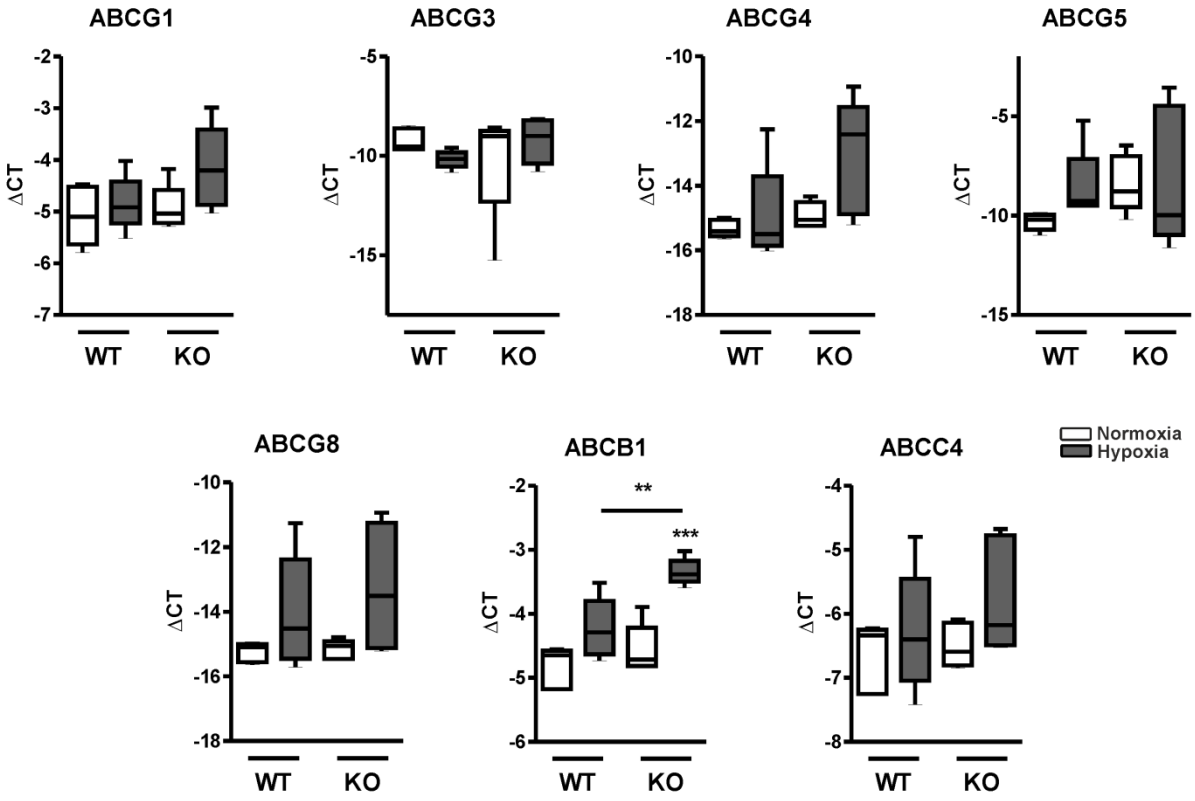

Figure 10. The expression of ABCG2-related ABC transporters in mouse lung homogenates

Relative mRNA expression of ABC transporters in lung homogenates of mice exposed to 4wks of hypoxia (10%) or normoxia (21%) were quantified by qPCR (ΔCT=CT housekeeping gene- CT gene of interest, n=5, **p <0.01, ***p <0.001).

Significant diastolic dysfunction in ABCG2 KO mice in response to hypoxia

Careful investigation of the hemodynamic pressure curves obtained from right heart catheterisation indicated a disturbance at the end-diastole in the case of ABCG2 knockout (KO) mice under hypoxia, manifested by an elevation of end-diastolic pressure (EDP) (*Figure 11*). In normoxia, the right ventricle pressure at the end of diastole (RVEDP) was comparable between KO and WT mice (1.12 ± 0.29mmHg vs. 1.69 ± 0.12mmHg) (*Figure 11B*), and hypoxia significantly increased this parameter in both KO and WT mice, compared to their normoxic counterparts (RVEDP p <0.001, *see Table 6*). This result is not surprising, considering that EDP has been shown to be elevated in clinical and experimental pulmonary hypertension (110-115).

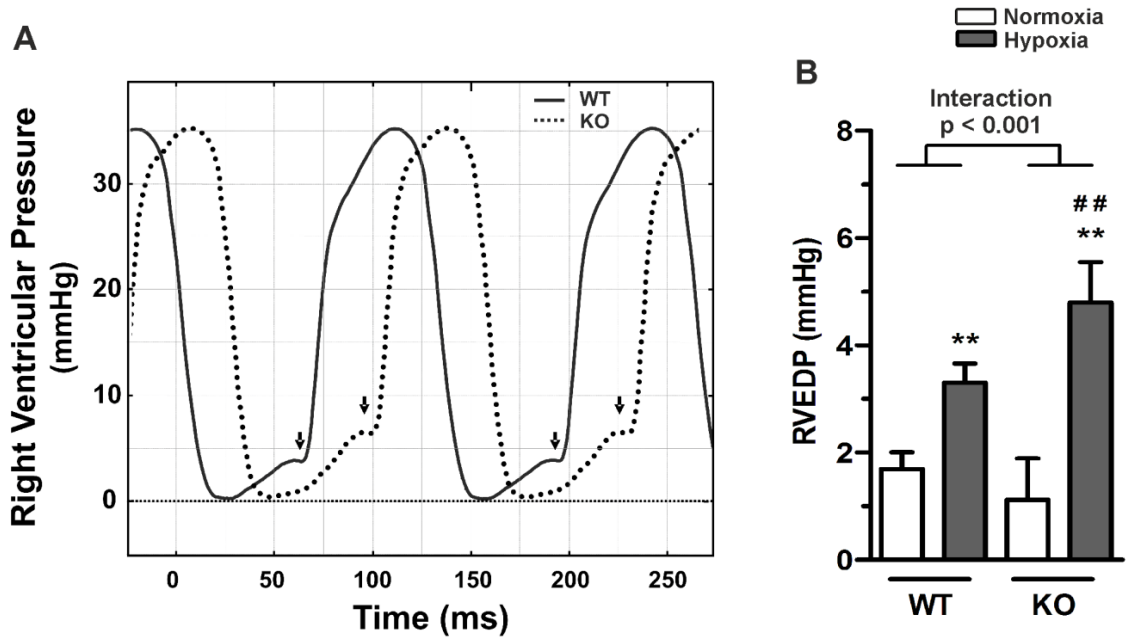

Figure 11. Elevated right ventricular end-diastolic pressure in ABCG2 KO mice in response to hypoxia

(A) Representative pressure curves showing right ventricular pressure recordings, illustrating (arrows) end-diastolic pressure alterations in ABCG2 KO (dashed line) compared to WT mice (continuous) under hypoxia. (B) Summarised haemodynamic parameters showing right ventricular end-diastolic pressure (RVEDP) (n= WT nox:7, WT HOX:7, KO nox:7, KO HOX:7) obtained from right ventricle of ABCG2 KO and WT mice exposed to normoxia or chronic hypoxia. Bar graphs represent values as means ±SD (Interaction p corresponds to hypoxia·genotype interaction, # corresponds to difference between genotypes in hypoxia, * corresponds to hypoxic treatment within genotype; *p <0.05, **p ##p <0.01). Figure modified from (102).

However, the RVEDP elevation was significantly stronger in KO animals than in WT mice, as it is demonstrated by the interaction of hypoxia and genotype (p for interaction <0.001, *Figure 11B*). It indicates that in ABCG2 KO mice hypoxia caused diastolic dysfunction. This dysfunction appeared to be relevant only in the late diastolic phase, as the time constant of ventricular pressure decay (Tau (τ)) – describing early diastolic conditions - did not differ between any of the experimental groups (*Figure 12A*). Furthermore, there was decreased mindP/dt in hypoxia in both genotypes (p <0.001, *Figure 12B*), however it is consistent with the ongoing pulmonary hypertension causing larger pressure decay in early diastole. Similarly, an increased maxdP/dt was observed as well (*Figure 12C, see Table 6*).

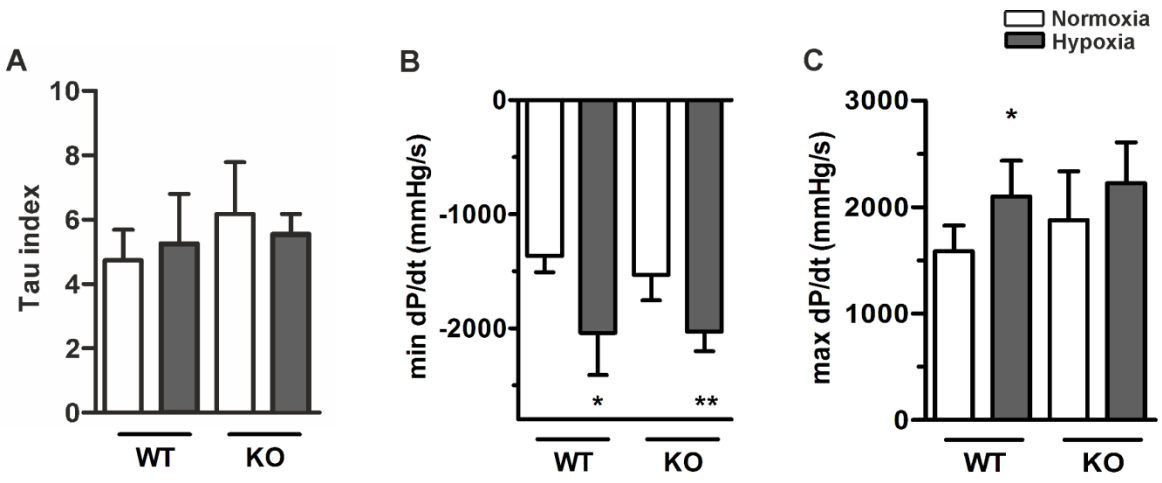

Figure 12. Hemodynamic parameters describing diastole in the mouse right ventricle

Summarised haemodynamic parameters showing (A) Tau index (n= WT nox:6, WT HOX:7, KO nox:7, KO HOX:7), (B) mindP/dt (n= WT nox:7, WT HOX:7, KO nox:7, KO HOX:7) and (C) maxdP/dt (n= WT nox:7, WT HOX:7, KO nox:7, KO HOX:7) obtained from right ventricle of ABCG2 KO and WT mice exposed to normoxia or chronic hypoxia. Bar graphs represent values as means ±SD (* corresponds to hypoxic treatment within genotype; *p <0.05, **p <0.01). Figure modified from (102).

Left ventricular end-diastolic pressure (LVEDP) was not different between WT and KO mice in normoxia but hypoxia caused an increase in this parameter (p =0.001, see *Table 6, Figure 13*). Despite the effect was more pronounced in ABCG2 KO mice, the interaction between hypoxia and genotype was not significant (p for interaction =0.11, *Figure 13B*), which can be due to the low sample size in these groups.

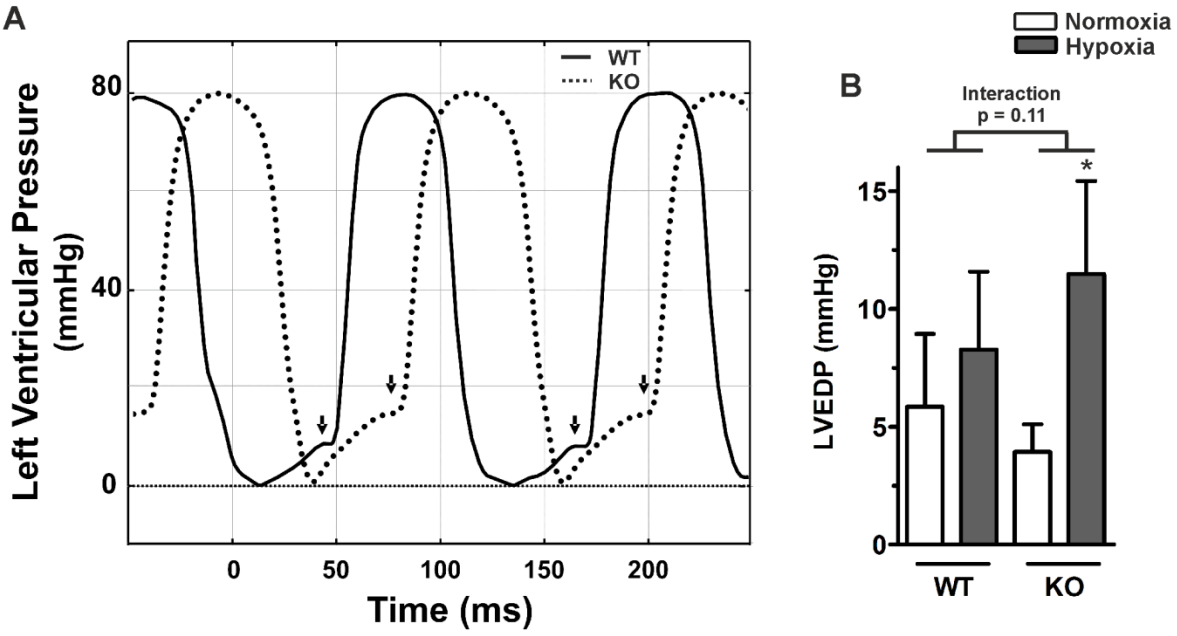

Figure 13. Elevated left ventricular end-diastolic pressure in ABCG2 KO mice in response to hypoxia

(A) Representative pressure curves showing left ventricular pressure recordings, illustrating (arrows) end-diastolic pressure alterations in ABCG2 KO (dashed line) compared to WT mice (continuous) under hypoxia. Summarised haemodynamic parameters showing (B) left ventricular end-diastolic pressure (LVEDP) obtained from left ventricle of ABCG2 KO and WT mice exposed to normoxia or chronic hypoxia. (n= WT nox:5, WT HOX:7, KO nox:5, KO HOX:6) Bar graphs represent values as means ±SD (* corresponds to hypoxic treatment within genotype; *p <0.05). Figure modified from (102).

Hypoxia had a significant effect on left ventricular mindP/dt independently of the genotype (p =0.013, *see Table 6*, *Figure 14B*). However, neither hypoxia nor genotype had any significant effects on maxdP/dt or Tau (*Figure 14A, C, see Table 6*). (Text modified from (102)).

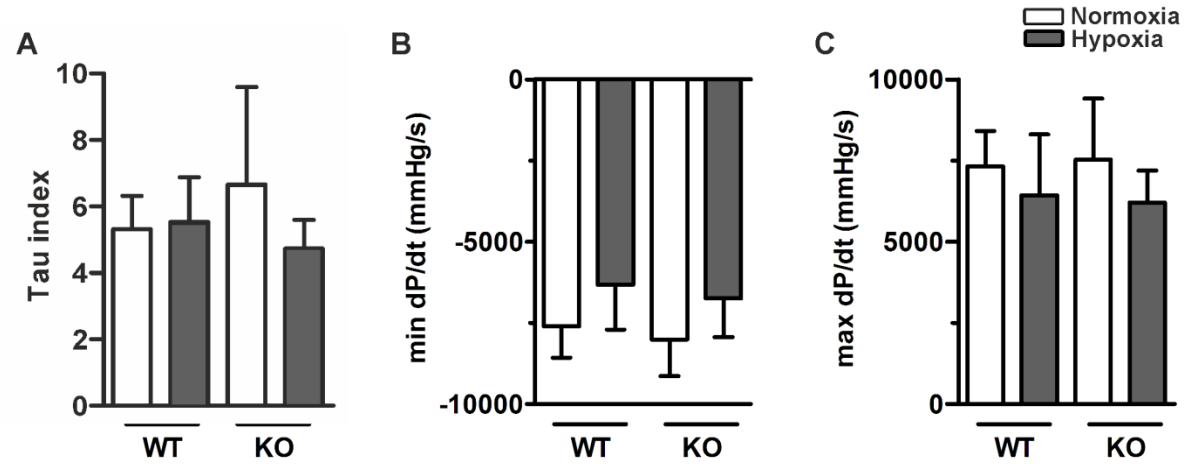

Figure 14. Hemodynamic parameters describing diastole in the mouse left ventricle
Summarised haemodynamic parameters showing (A) Tau index, (B) mindP/dt and (C) maxdP/dt obtained from left ventricle of ABCG2 KO and WT mice exposed to normoxia or chronic hypoxia. (n= WT nox:5, WT HOX:7, KO nox:5, KO HOX:6) Bar graphs represent values as means ±SD. Figure modified from (102).

Increased ventricular fibrosis in ABCG2 KO mice under hypoxia, without changes in capillary density

Alterations in myocardial tissue composition can greatly influence diastolic function (116). If massive collagen deposition occurs, it directly increases the extracellular matrix-mass in the ventricles. This increases passive tissue stiffness, which manifests in elevated EDP. Therefore, in the following step, we investigated ventricular fibrosis, measured by collagen deposition in the myocardium. In normoxia, the mice did not show differences in right- (*Figure 15*) or left ventricular fibrosis (*Figure 16*).

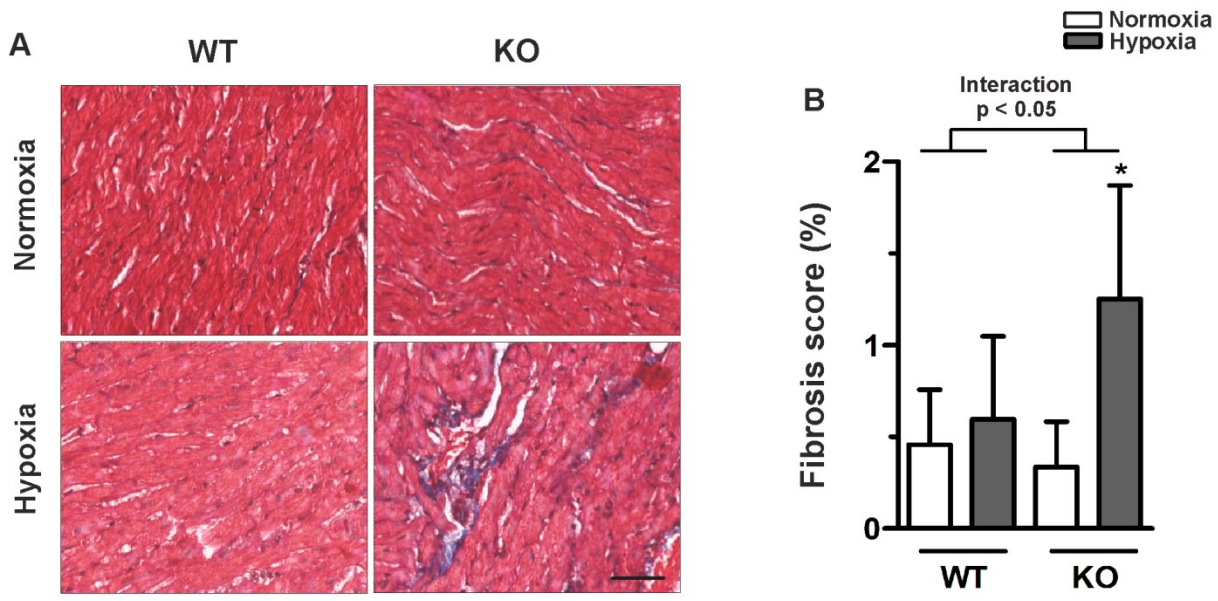

Figure 15. Increased right ventricular fibrosis in ABCG2 KO mice under hypoxia

(A) Masson`s trichrome staining shows presence of collagen (blue) in right ventricular sections of ABCG2 KO and WT mice after normoxic or hypoxic exposure. (B) Quantification shows presence of collagen in the right ventricle. (n= WT nox:6, WT HOX:7, KO nox:7, KO HOX:7) Scale bar indicates 50µm. Bar graphs represent values as means ±SD (Interaction p corresponds to hypoxia·genotype interaction, * corresponds to hypoxic treatment within genotype; *p <0.05). Figure modified from (102).

Hypoxia, however significantly increased the ventricular fibrosis in ABCG2 KO, but not in WT mice. This was the case in both right and left ventricles (RV p for interaction <0.05; LV p for interaction <0.01). In the RV, the collagen deposition was in general more pronounced, as indicated by higher fibrosis score, but the hypoxia-induced changes in the KO mice was identical in both ventricles. It seems that the fibrosis score followed the same response pattern as it was observed in the case of EDP, indicating a relationship between these two parameters. This is further supported by a significant correlation between RV fibrosis and RVEDP in ABCG2 KO mice ($p < 0.05$, $R^2 = 0.59$, *Figure 17A*). This correlation was not present in the left ventricle (*Figure 17B*).

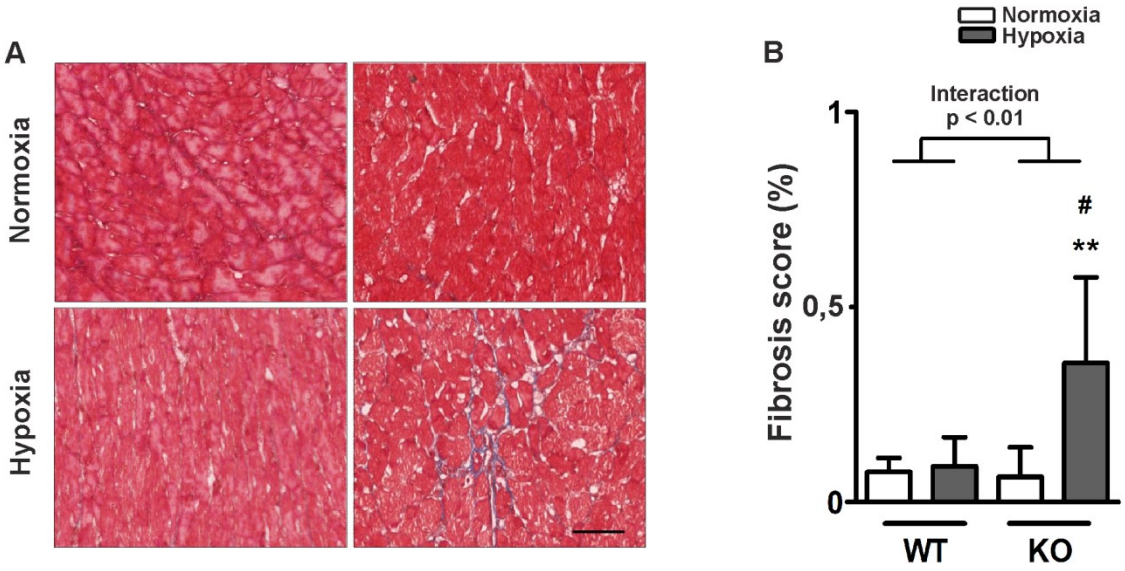

Figure 16. Increased left ventricular fibrosis in ABCG2 KO mice under hypoxia

(A) Masson`s trichrome staining shows presence of collagen (blue) in left ventricular sections of ABCG2 KO and WT mice after normoxic or hypoxic exposure. (B) Quantification shows presence of collagen in the left ventricle. (n= WT nox:6, WT HOX:7, KO nox:7, KO HOX:7) Scale bar indicates 50µm. Bar graphs represent values as means ±SD (Interaction p corresponds to hypoxia·genotype interaction, # corresponds to difference between genotypes in hypoxia, * corresponds to hypoxic treatment within genotype; #p <0.05, **p <0.01). Figure modified from (102).

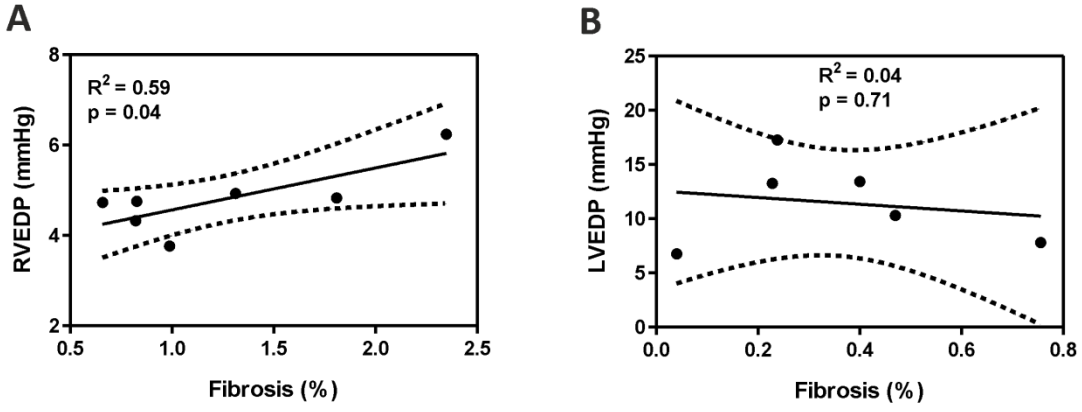

Figure 17. Correlation of ventricular EDP with ventricular fibrosis in ABCG2 KO hypoxic mice.

The acquired (A) RVEDP and (B) LVEDP values were correlated with fibrosis score obtained from the right ventricles (n= 7) and left ventricles (n=6) –respectively- of hypoxic ABCG2 KO mice.

As the lack of ABCG2 resulted in collagen deposition in the heart under hypoxia, we wanted to know if the same is true for the lungs. When we determined fibrotic content of the lungs, we observed that neither hypoxia, nor the lack of ABCG2 had any significant effect on lung fibrosis (*Figure 18*).

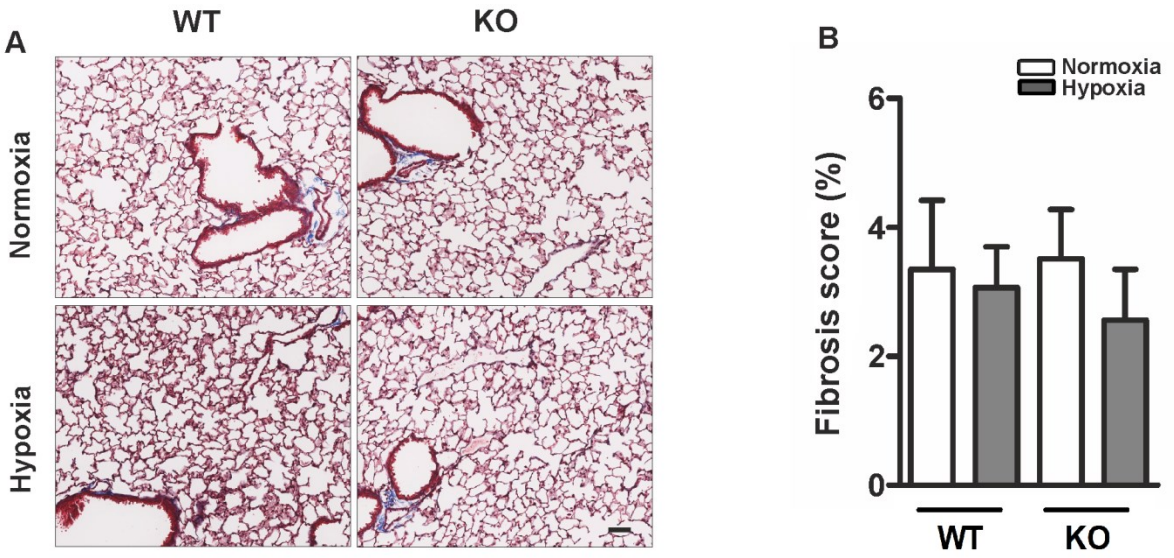

Figure 18. Unaffected lung fibrosis in the experimental mice

(A) Masson`s trichrome staining shows presence of collagen (blue) and (B) quantification in lung tissue sections of ABCG2 KO and WT mice after normoxic or hypoxic exposure. (n= WT nox:9, WT HOX:9, KO nox:9, KO HOX:9) Scale bar indicates 50µm. Bar graphs represent values as means ±SD. Figure modified from (102).

It has been shown, that during ventricular hypertrophy, the number of cardiac capillaries can influence contractile function and apoptosis of cardiomyocytes, which can be a precedent of fibrosis (117). Additionally, previous studies showed that mice lacking ABCG2 have reduced angiogenesis in the LV upon transverse aortic constriction . To investigate if the lack of ABCG2 influenced ventricular capillary density in our experimental setup, we visualized capillaries in the ventricles using thrombomodulin (*Figure 19*).

After analysing the capillary density, it became evident, that neither hypoxia, nor the lack of ABCG2 had any effect on ventricular capillary density (*see Table 6*). This indicates that the observed EDP elevation and ventricular fibrosis may occurred independently of ventricular angiogenesis. (Text modified from (102)).

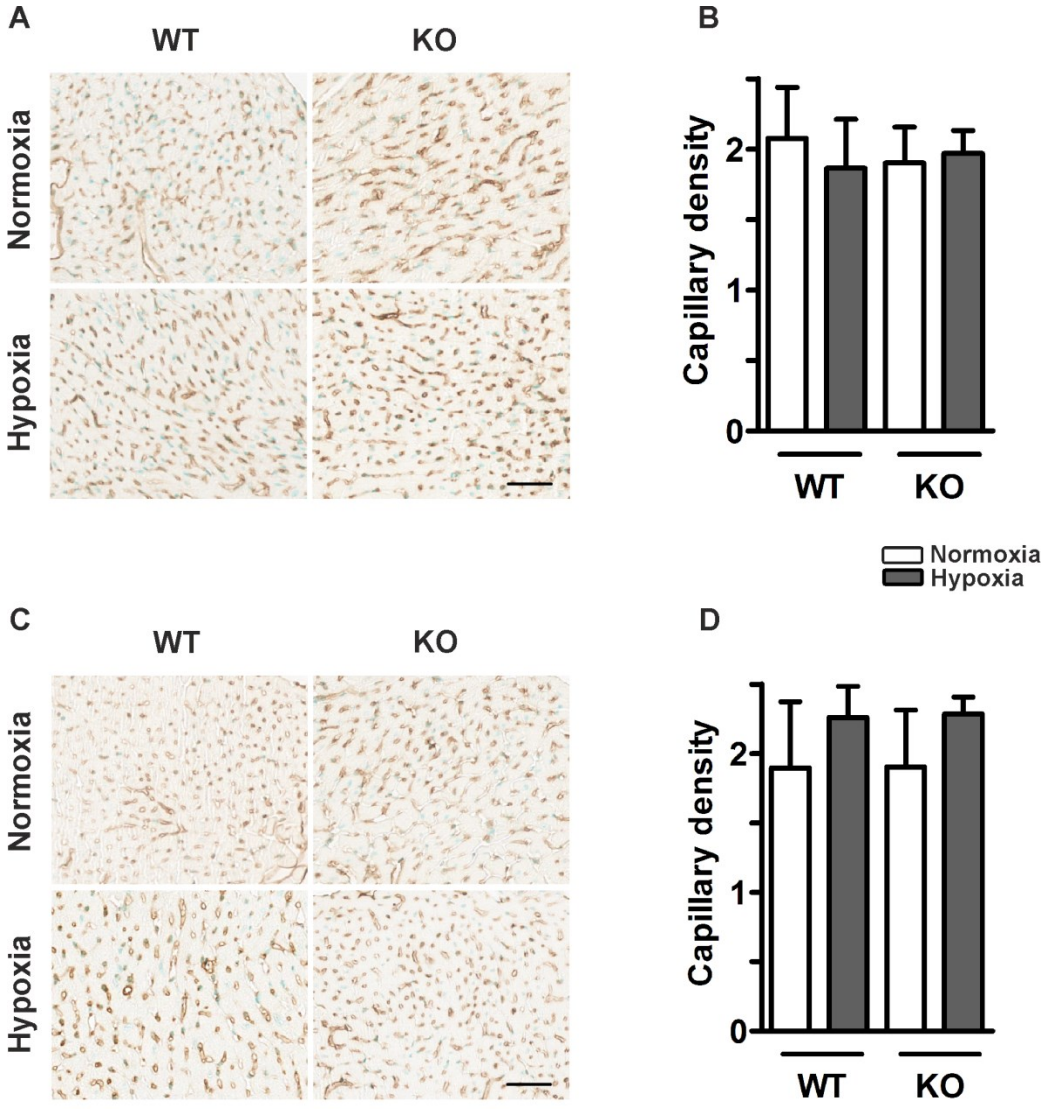

Figure 19. Comparable ventricular capillary density in WT and ABCG2 KO mice

Capillaries are visualized by thrombomodulin staining in ABCG2 KO and WT right (A) and left ventricles (C) of mice exposed to normoxia or chronic hypoxia. Quantification of capillary density in the RV and LV are shown in subset (B) and (D) respectively (n= WT nox:7, WT HOX:7, KO nox:7, KO HOX:6). Figure modified from (102).

Fibrosis-related genes in ventricular tissue of hypoxic mice

We have shown that under hypoxia, fibrotic deposition was present in both ventricles of the knockout animals. We were also interested, if any ongoing fibrotic processes can be detected at the end of the treatment, therefore we investigated the expression of fibrosis-related genes by quantitative real-time PCR in the RV and LV (*Figure 20*). At the end of 4 weeks hypoxia, when myocardial fibrosis was already established, there were no significant changes in most of the investigated genes. Only collagen type III alpha 1 (Col3A1) was significantly upregulated in the RV of ABCG2 KO mice in hypoxia ($p < 0.05$). The persistent activation of Col3A1 could be due to both hypoxia and increased RV afterload, however as there was no such increase in the LV, this indicates that the ongoing upregulation was mainly due to the presence of increased afterload.

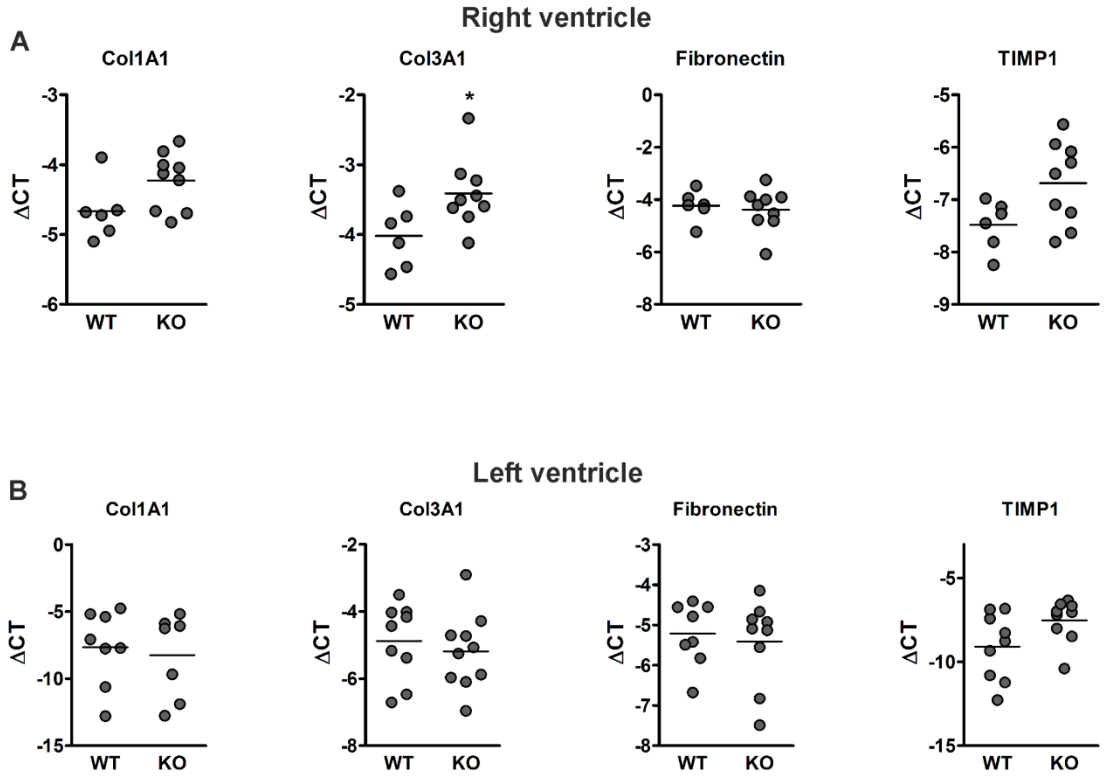

Figure 20. Fibrosis-related genes in mouse ventricular tissue after 4 weeks of hypoxia

Graphs show Collagen1A1, Collagen3A1, Fibronectin and TIMP1 mRNA expression in the (A) right and (B) left ventricles of WT and KO mice after exposure of 4 weeks chronic hypoxia. ($n \geq 6$ for each group, * corresponds to hypoxic treatment, $^*p<0.05$). Figure modified from (102).

Increased extracellular matrix production in ABCG2-silenced mouse isolated cardiac fibroblasts under hypoxia.

The regulation of collagen matrix-content in the myocardium is primarily dedicated to cardiac fibroblasts (98). For this reason, we wanted to know if cardiac fibroblasts do express ABCG2, and if they have any dependency of this transporter.

Using fibroblastic marker (vimentin), we visualized cardiac fibroblasts in the mouse ventricular tissue, and simultaneously stained for ABCG2 as well (*Figure 21*). ABCG2 was present in those cells, having positive staining for vimentin, which indicated, that cardiac fibroblasts do express ABCG2.

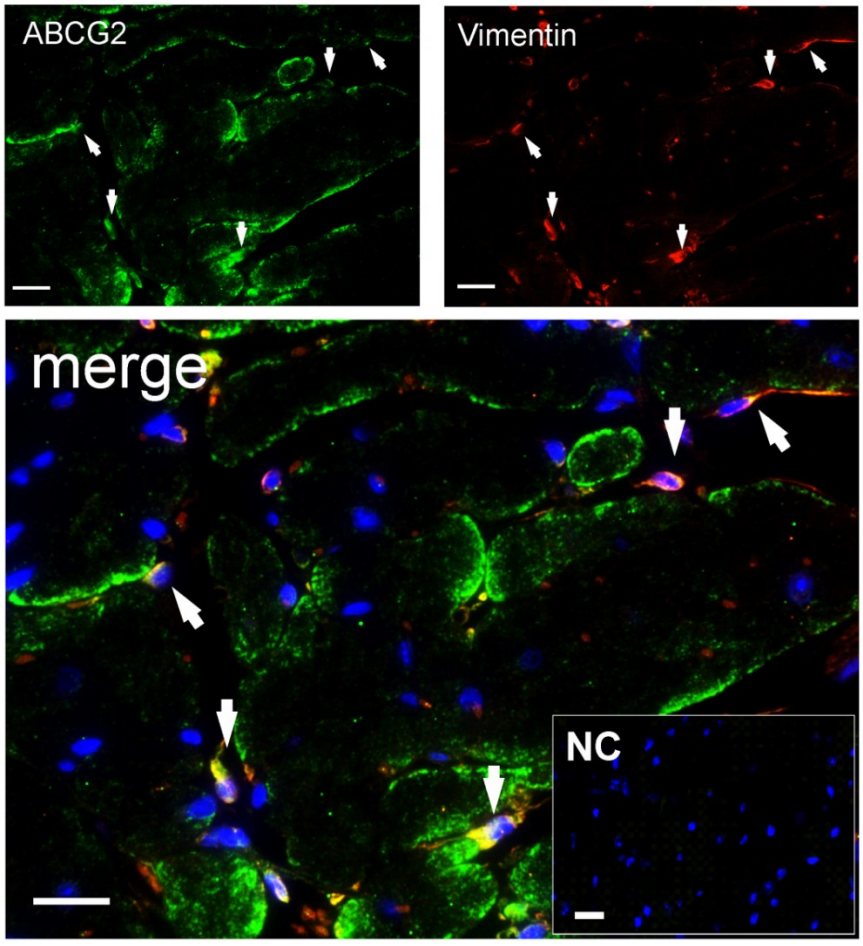

Figure 21. Presence of ABCG2 in the mouse ventricle

(A) Fluorescent immunostainings indicate ABCG2 (green) and vimentin (red), and an overlaid picture (merge) with DAPI nuclear staining (blue) in the mouse ventricle. Arrows pointing out cardiac cells coexpressing ABCG2 and vimentin. Inset represents correspondent negative control. Scale bar = 20 μm. Figure modified from (102).

Next, we isolated cardiac fibroblasts from the mouse ventricles. The efficiency of the isolation was validated by immunofluorescence, showing that the cells are expressing various fibroblastic markers (vimentin, periostin, S100A4, fibronectin). F-actin staining provided information about the overall cell shape and -structure (*Figure 22*).

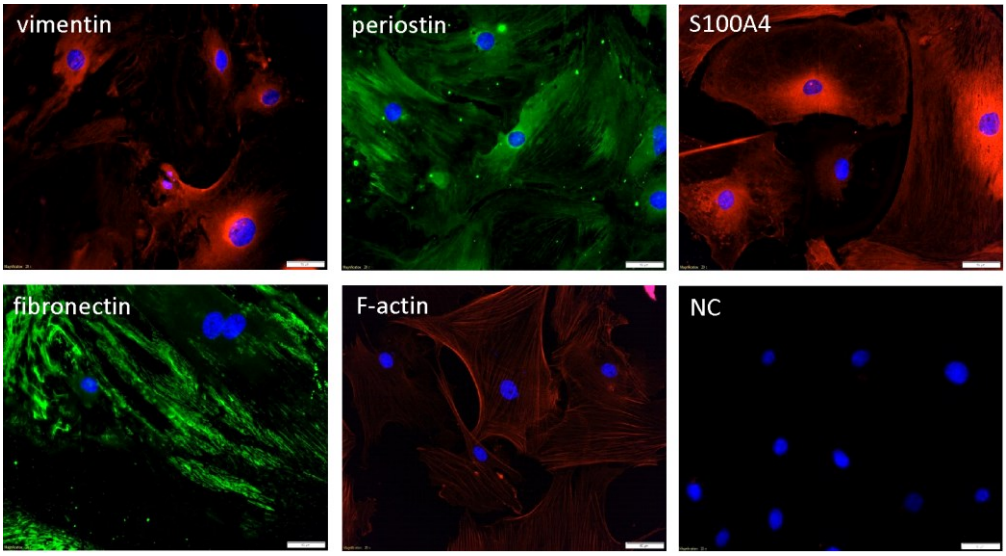

Figure 22.Characterisation of isolated mouse cardiac fibroblasts

Immunofluorescence images display F-actin staining and positive staining for characteristic markers in fibroblasts isolated from mouse ventricles. NC corresponds to negative control. Scale bar= 50µm. Figure modified from (102).

When we silenced the expression of ABCG2, cardiac fibroblasts showed increased collagen production under hypoxia ($p < 0.05$), mimicking the same result we observed before on cardiac fibrosis *in vivo*.

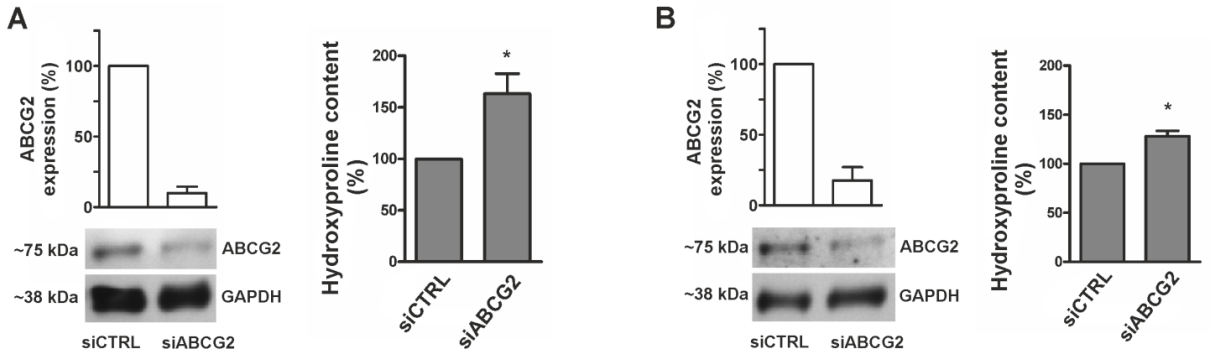

Figure 23. Collagen production in ABCG2 silenced mouse isolated cardiac fibroblasts under hypoxia

Graphs represent ABCG2 mRNA expression in mouse primary fibroblasts derived from (A) right ventricles and (B) left ventricles, after transfection with control siRNA or siABCG2 (n=3). Western blot gel pictures represent

protein levels of ABCG2. Collagen production is shown as Hydroxyproline content (%) in the correspondent fibroblasts (n=4). Bar graphs represent values as means ±SD (*p <0.05). Figure modified from (102).

On the other hand, when we repeated the experiments with fibroblasts derived from the lungs of the same mice, they did not show extracellular matrix production upon silencing of ABCG2 in hypoxia (*Figure 24*). These results suggest that in hypoxic mouse ventricular fibroblasts, -but not in pulmonary fibroblasts- ABCG2 protects against excess collagen production, recapitulating the previously observed *in vivo* conditions. (Text modified from (102)).

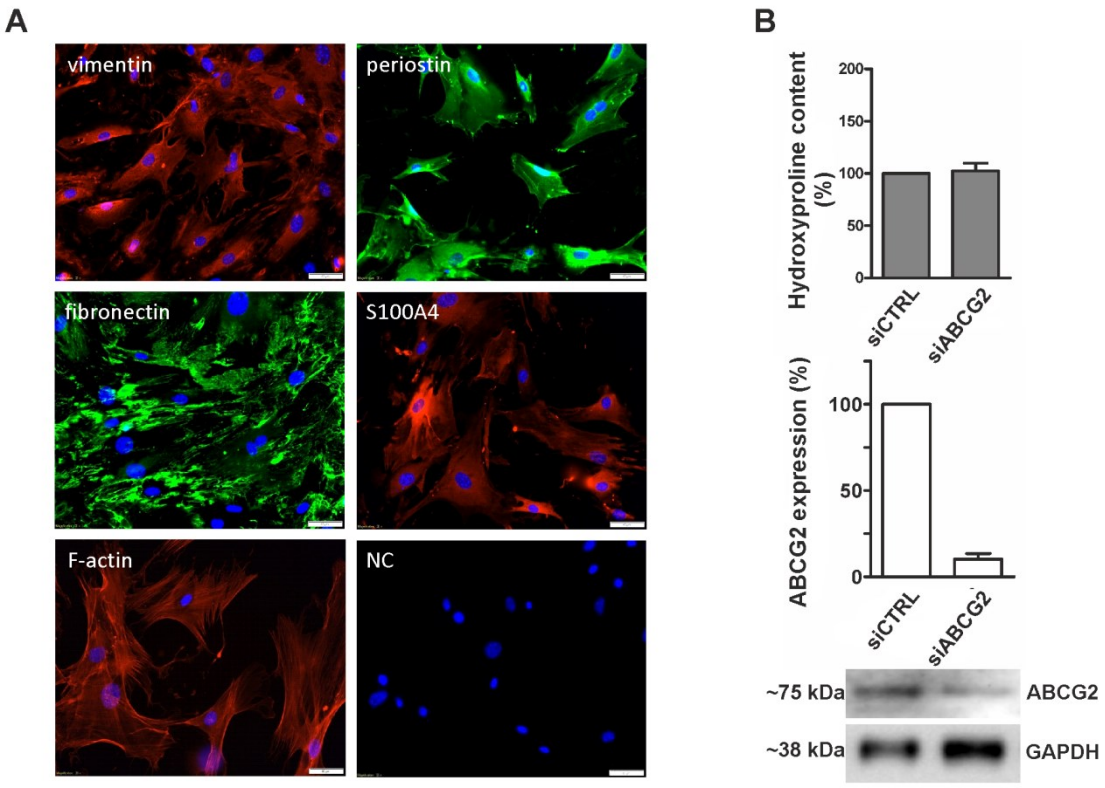

Figure 24. Unaltered collagen production in ABCG2 silenced mouse isolated lung fibroblasts under hypoxia
(A) Immunofluorescence images display F-actin staining and positive stainings for characteristic markers in fibroblasts isolated from mouse lungs. NC corresponds to negative control. Scale bar= 50µm. (B) Graphs represent collagen content as Hydroxyproline percentage in these cells (n=4), and ABCG2 mRNA expression, after transfection with control siRNA or siABCG2 (n=3). Western blot gel pictures represent protein levels of ABCG2. Bar graphs represent values as means ±SD. Figure modified from (102).

Increased extracellular matrix production in ABCG2 silenced human primary cardiac fibroblasts under hypoxia.

To investigate if the observed results could be extrapolated into humans as well, in the following steps we used human primary cardiac fibroblasts, and we demonstrated the first time, that these cell types express ABCG2 (*Figure 25*). Using small interfering RNA-technique against ABCG2, we reached nearly 80 percent silencing efficiency of the transporter (*Figure 25B*).

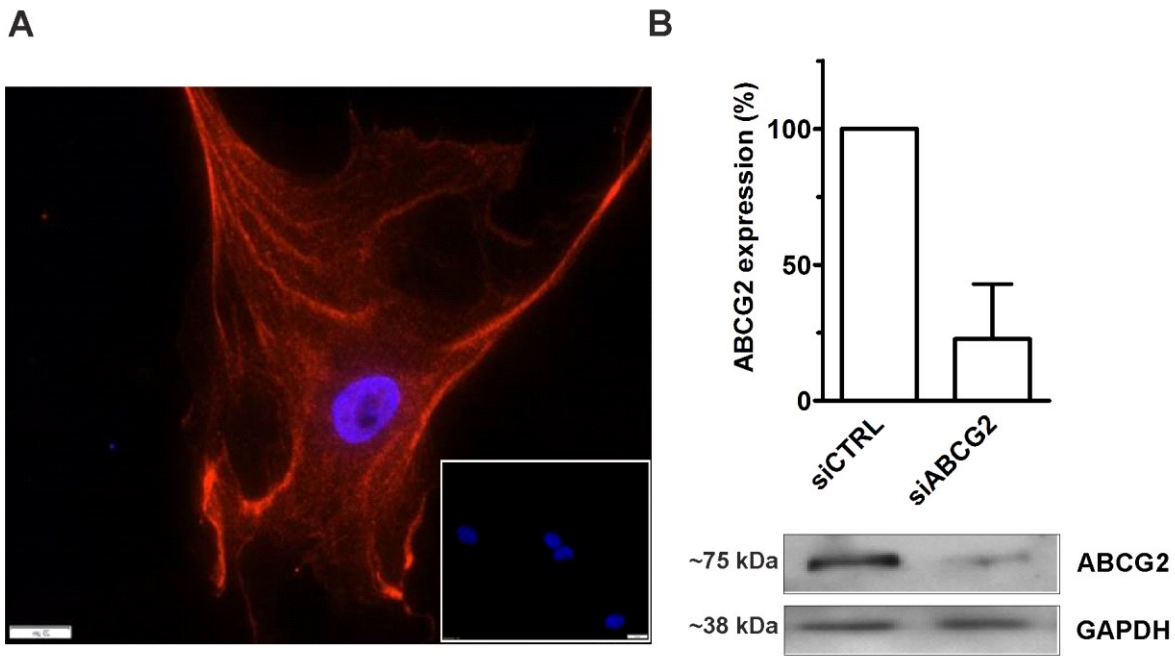

Figure 25. Presence of ABCG2 in human primary cardiac fibroblasts

(A) Fluorescent immunostaining indicate ABCG2 (red) and DAPI nuclear staining (blue) in human cardiac fibroblast. Insert represents correspondent negative control. Scale bar= 20 µm. (B) Bar graph shows ABCG2 mRNA expression in human primary cardiac fibroblasts transfected with either control siRNA or siABCG2 (n=3). Western blot gel picture represents protein levels of ABCG2 in human primary cardiac fibroblasts. Equalized loading was confirmed with GAPDH. Figure modified from (102).

When ABCG2 was supressed, there was an increased collagen production under hypoxia in human cardiac fibroblasts, showing significant interaction between the treatment and ABCG2 silencing (p for interaction <0.05, *Figure 26A*). This again recapitulated the mouse *in vivo* and *in vitro* conditions, and indicated that in human primary cardiac fibroblasts ABCG2 plays a protective role against hypoxia-induced collagen production.

Since excess tissue collagen can be the result of a raised number of cardiac fibroblasts in the ventricle, we have included proliferation measurement investigating the dynamic change in cardiac fibroblast-numbers, upon our treatment. The proliferation assay showed that neither hypoxia, nor the silencing of ABCG2 had any significant effect on human primary cardiac fibroblast-numbers (*Figure 26B*). (Text modified from (102)).

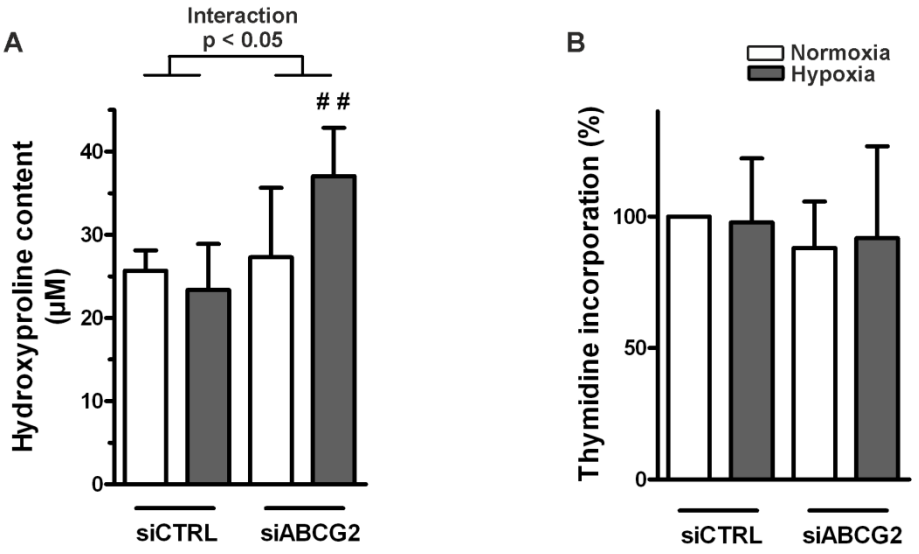

Figure 26. Increased collagen production in ABCG2 silenced human primary cardiac fibroblasts under hypoxia
(A) Graphs represent collagen content in human primary cardiac fibroblasts, measured by hydroxyproline assay (n=5). (B) Human primary cardiac fibroblast proliferation, measured by [3H]thymidine incorporation (n=4). Bar graphs represent values as means ±SD (Interaction p corresponds to hypoxia·genotype interaction, # corresponds to difference between genotypes in hypoxia, ##p <0.01). Figure modified from (102). Figure modified from (102).

Circulating cytokines in the hypoxic mice

We were also interested if the cytokine milieu was altered in the absence of ABCG2 under hypoxia. For this purpose, we measured a variety of circulating cytokines and chemokines in the serum of our experimental animals. Out of 40 investigated cytokines, the circulating levels of IL-1ra, MCP-1, G-CSF and CXCL1 showed significant elevation in ABCG2 KO mice under hypoxia (*Figure 27*).

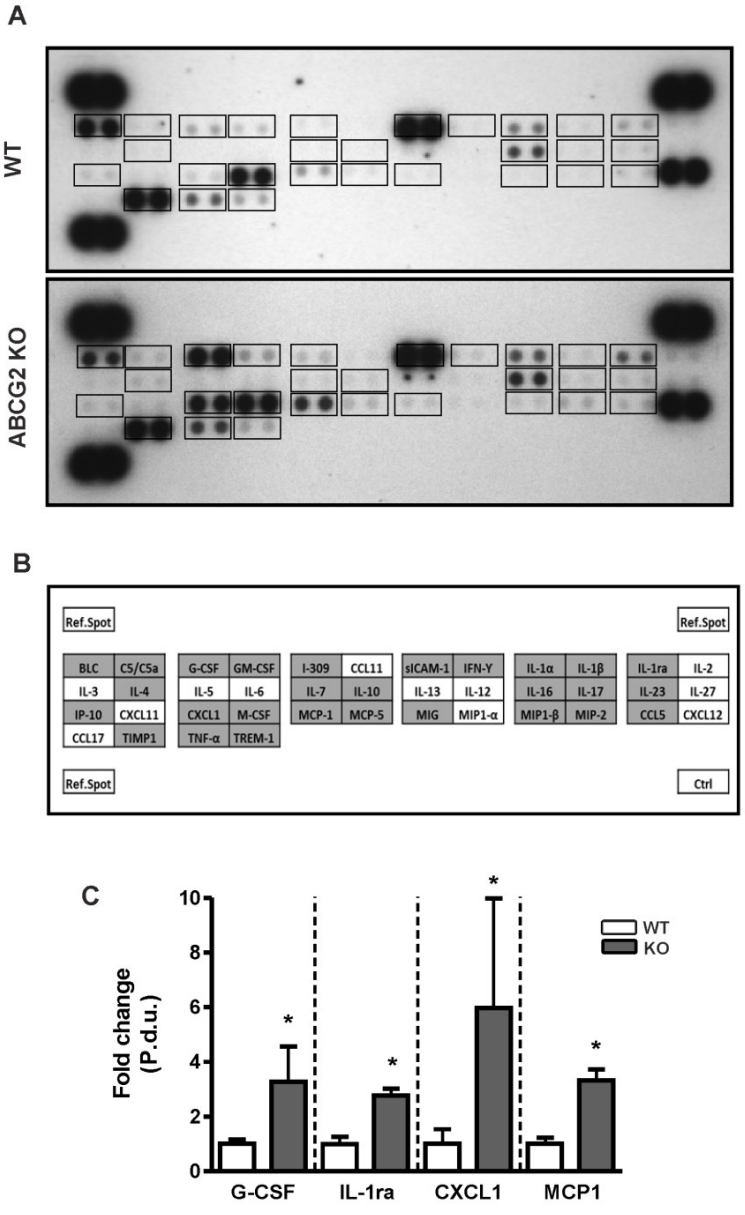

Figure 27. Increased level of fibrosis-associated cytokines in hypoxic ABCG2 KO mice

(A) Representative images show nitrocellulose-based mouse cytokine/chemokine array membranes performed on serum samples from hypoxia-treated WT and ABCG2 KO mice, (B) the position of each cytokine in the

membrane. (C) The correspondent pixel densities normalized to the given reference spots on the membranes are shown as means ±SD (n= 4) (*p <0.05). Figure modified from (102).

These cytokines has been shown to be linked to fibrosis (118-121). This suggests, that beside the direct effect of ABCG2 on cardiac fibroblasts – regarding excess collagen production-, the presence of a profibrotic cytokine-environment might have also favoured ventricular collagen deposition in ABCG2 KO mice under hypoxia.

Regulation of ABCG2 in the stressed mouse ventricle.

To gain information about the regulation of ABCG2 in the ventricles, we investigated chronic hypoxia treated mice. After establishment of pulmonary hypertension and cardiac fibrosis, ABCG2 was upregulated in the mouse right ventricles, but not in the left ventricles (*Figure 28*).

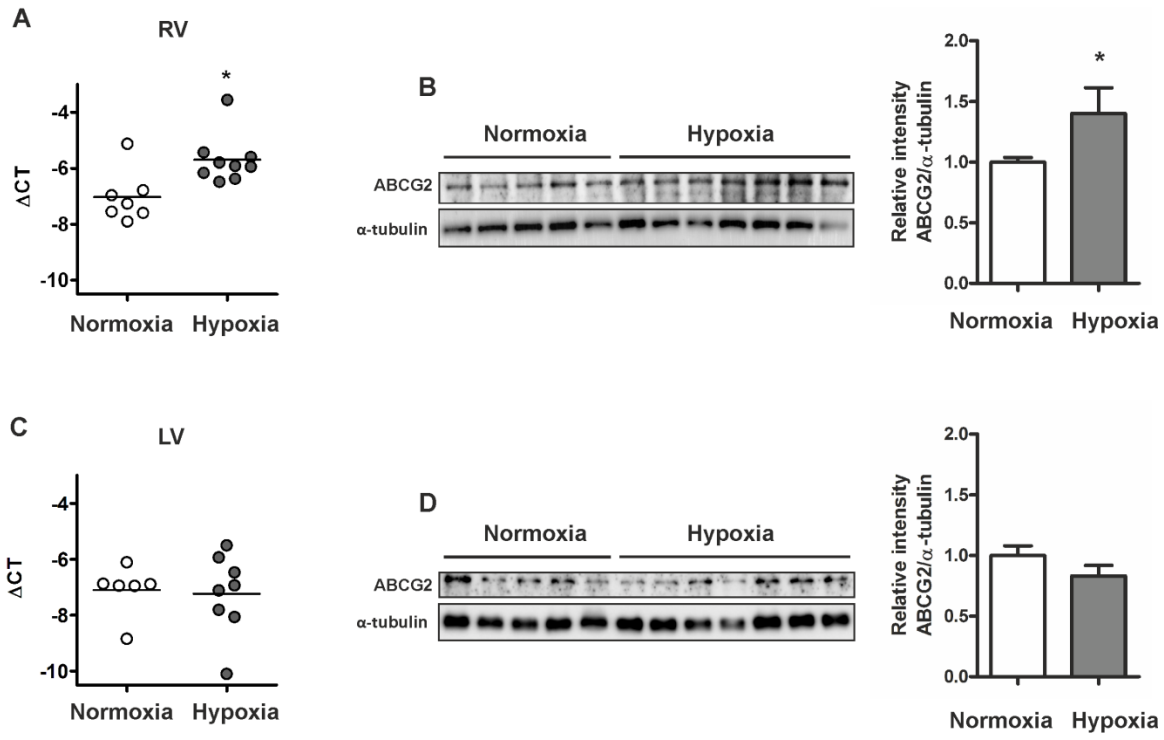

Figure 28. Regulation of ABCG2 in the stressed mouse ventricle

ABCG2 gene expression in (A) right - and (C) left ventricles of hypoxic mice (n≥6 for each group). Western blot analysis of ABCG2 in (B) right- and (D) left ventricles from mice after 4 weeks hypoxia (n= nox:5 , HOX:7). Signal densities were quantified using densitometric analysis. Bar graphs represent values as means ±SD (*p <0.05). Figure modified from (102).

These results suggested that it is not hypoxia, rather increased afterload which regulates ABCG2 in the myocardium. This notion was supported by the results gained from pulmonary arterial banded (PAB) mice, showing ABCG2 gene-upregulation (*Figure 29*). (Text modified from (102)).

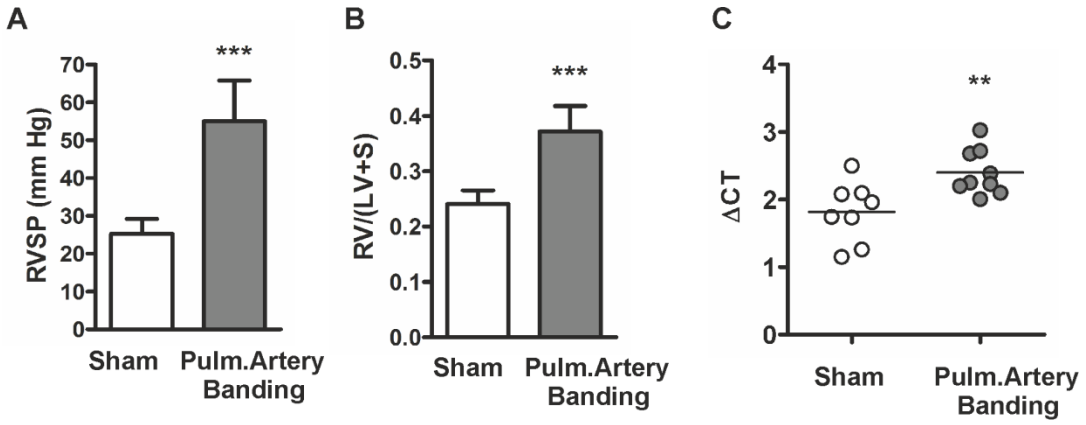

Figure 29. ABCG2 regulation in pulmonary artery banded right ventricle

(A) RV systolic pressure and (B) RV hypertrophy in sham operated and pulmonary artery banded (PAB) mice (n= Sham:8, PAB:9). (C) ABCG2 gene expression in right ventricles of PAB mice. Bar graphs represent values as means ±SD (**p <0.01, ***p <0.001). Figure modified from (102).

Discussion

In the present study we investigated the possible contribution of the ABC membrane transporter family member - ABCG2 to the development of pulmonary hypertension, and the importance of ABCG2 in the stressed myocardium.

Previous studies have shown that disturbances in the function of certain ABC transporters are linked to different pulmonary diseases, indicating their important role in lung physiology (33,34). More importantly, a recent study has shown that a particular member of ABC transporters directly contributes to the development of PH (35). Here we were focusing on ABCG2, an ABC transporter having not received attention so far in the field of pulmonary hypertension.

Our results showed that -amongst other ABC members, ABCG2 was highly regulated in the lungs of IPAH patients, and showed the presence in PASMCs and vascular endothelial cells, both playing a crucial role in the pathogenesis of the disease. Therefore we investigated, how PDGF –an important proliferative factor causing pulmonary vascular remodelling, influences ABCG2 expression in these cell types, and how the inhibition of ABCG2 affects the behaviour of these cells. ABCG2 was regulated by PDGF in PASMCs, and the inhibition of ABCG2 abolished PDGF-induced proliferation. The inhibition of ABCG2 resulted in the suppression of proliferation most likely because of the blockage of cell cycle, as it has been shown in smooth muscle cells. However, these results remained preliminary, therefore we cannot exclude that other processes play an important role. As proliferation of pulmonary arterial smooth muscle cells is one of the main characteristics of PH, ABCG2 might play an important role for the development of this disease.

To investigate ABCG2 *in vivo*, we have applied the hypoxia-induced pulmonary hypertension-mouse model. In this model, the chronic application of low oxygen levels inhibits the vasodilatative signalling pathways and leads to sustained pulmonary arterial vasoconstriction and remodeling, which ultimately leads to PH (122). ABCG2 showed strong upregulation in the lungs of pulmonary hypertensive mice, indicating that the transporter might be important for the disease. However, when we subjected ABCG2 knockout mice to chronic hypoxia, they developed the same elevated right ventricular pressure and hypertrophy as

wild type animals. Thus the absence of ABCG2 had no effect on the development of PH. As an explanation for this discrepancy, we have hypothesized, that another structurally- and/or functionally related ABC transporter might have compensated for the disruption of ABCG2 under hypoxia. Thus, it seemed relevant to compare gene expression of other ABC transporters in ABCG2 KO and wild type lungs under hypoxia. Indeed, ABCB1 transcripts showed high levels of upregulation in the absence of ABCG2, suggesting that in the lung, ABCB1 might act synergistically with ABCG2, and may compensate for the lack of ABCG2. This notion is further supported by the findings, that ABCB1 and ABCG2 have a certain degree of substrate overlap (109).

On the other hand, ABCG2 knock out mice showed severe alterations in the heart. They developed significant biventricular diastolic dysfunction and fibrosis under chronic hypoxia but not under normoxic conditions. Exposure of mice to chronic hypoxia is reminiscent of many of the anatomic and hemodynamic alterations that are known from humans with chronic lung disease (123,124). After development of pulmonary arterial remodelling, the RV has to cope with an increased afterload which initially results in the elevation of systolic and diastolic ventricular pressures, leading to RV hypertrophy and finally to RV decompensation (23,90,125-127). Incomplete ventricular relaxation at end-diastole causes elevated filling pressure which is the main characteristic of diastolic dysfunction. In the LV, elevated ventricular end-diastolic pressure is a well-established indicator of heart failure and predictor of mortality (128). When ABCG2 KO mice were exposed to chronic hypoxia, we observed increased ventricular fibrosis and an overt worsening of biventricular diastolic function, as demonstrated by a significant increase in EDP of both cardiac chambers.

Previous studies in the transverse aortic constriction model had shown that mice lacking ABCG2 have reduced angiogenesis in the LV which was associated with cardiac hypertrophy (80,81). However, our results indicated that neither hypoxia nor the lack of ABCG2 had any effect on ventricular capillary density. This indicates that the observed alterations in diastole may be independent of angiogenesis.

The left ventricular expression of the ABCG2 transporter in human heart failure is strongly elevated and is correlated with the atrial natriuretic peptide (ANP) level (79). In addition,

genetic disruption of ABCG2 worsens cardiac remodelling and mortality of mice after myocardial ischemia, as well as after transverse aortic constriction (TAC)(80,81). Furthermore, hypoxia enhances the transcription of ABCG2 via hypoxia inducible factor (HIF). A very elegant study suggested that ABCG2 protects from hypoxia by preventing the accumulation of porphyrins, explaining why the lack of ABCG2 increases the sensitivity to hypoxia (42). In line with this, we found significantly increased ABCG2 levels in the RV of chronic hypoxic pulmonary hypertensive mice, indicating a putative role of this transporter in the stressed heart. It is likely that in the hypoxic heart the lack of ABCG2 leads to an accumulation of metabolic products, directly triggering collagen production. Nevertheless, we cannot exclude other possible contributing mechanisms. ABCG2 is also a marker of side population stem cells (SPSC), allowing these cells to maintain their stem cell-ness (53,54). The heart harbours resident SPSCs, able to differentiate into several cell types (129,130). It has been shown recently that ABCG2 modulates cardiac SPSC cycle progression and asymmetric cell division (77). ABCG2 activation after cardiac injury could restore and increase progenitor cell numbers, whereas inhibition of the transporter and activation of asymmetric cell division of cardiac progenitors might promote tissue regeneration. Therefore, myocardial fibrosis could also occur due to impairment of the formation of myocardial progenitor cells. Other studies detected ABCG2 expression in cardiomyocytes, raising the possibility that deletion of the transporter might have a direct effect on cardiomyocytes, which could contribute to a defective ventricular performance under hypoxia (78). Impaired cardiomyocyte function is usually a consequence of disturbed intracellular Ca^{2+} homeostasis. The rate of Ca^{2+} removal from the cytosol is the major regulator of diastolic relaxation, and any interfering process can potentially delay this process. This includes alterations in calcium-handling protein function, like sarcoplasmic reticular Ca^{2+}-ATPase (SERCA) or its inhibitory protein phospholamban (131,132). During relaxation, SERCA actively transfers the Ca^{2+} from the cytosol to the sarcoplasmic reticulum at the expense of ATP. When phospholamban is associated with SERCA, the rate of this cytosolic Ca^{2+} decay is reduced, leading to prolongation of myocardial relaxation. It follows that overexpression of SERCA or inhibition of phospholamban improves diastolic function (133). In addition to SERCA, the Na^{+}/Ca^{2+} exchanger (NCX) also contributes

to diminish the amount of cytosolic Ca^{2+}. NCX is a high capacity Ca^{2+} transporter, able to extrude 5000 Ca ions per second, thus playing an important role in the regulation of diastolic function. Its dysfunction may considerably impair myocardial relaxation (134,135). However, despite the identification of molecular mechanisms involved in cardiomyocyte relaxation, their direct impact on diastolic function remains still unclear (136). Relaxation delay has a major effect on the early stage of diastole, however, it is still under debate what is its effect on late diastolic function. Rather the passive components of the myocardium can influence the late diastolic phase. If myocardial collagen content increases, it leads to elevated passive tissue stiffness, having an impact on late diastole, manifested as elevated EDP (90,95-97). In our experiments, parameters describing early diastolic relaxation -such as Tau-index or min dP/dt- remained unchanged between genotypes. This indicates that in our model, there were no disturbances in myocyte-calcium handling protein function, because this would result in a delay in the first phase of diastole, which would lead to increased Tau and min dP/dt. Instead, we have seen an elevation in end-diastolic pressure, an indicator of diastolic dysfunction and heart failure (128,137). This can be caused by excess myocardial fibrosis which may lead to functional changes of the ventricle (116). Similar to our findings, previous reports in both animal models and humans had shown a relationship between the degree of cardiac fibrosis and diastolic dysfunction (84,138-144). The myocardium consists of myocytes harboured in a supportive fibrillar connective tissue network, composed largely of collagen. Extracellular matrix deposition may provide a cardioprotective effect by increasing myocardial structural resistance, protecting against elevated pressure (145). However, extracellular matrix accumulation can decrease ventricular performance (91). Elevated myocardial fibrosis is one of the main pathological features associated with diastolic heart failure (90,116). Furthermore, therapies ameliorating ventricular fibrosis have been shown to improve diastolic function (139,146). Our study shows that the hypoxia-induced changes in the ventricular myocardium are markedly exaggerated in ABCG2 KO mice suggesting that ABCG2 protects from hypoxia-induced myocardial fibrosis. Interestingly, the same response pattern was found in the right and left ventricle although the left ventricle is clearly not affected by increased afterload in chronic hypoxia. This suggests that hypoxia *per se* and not

hypoxia-induced changes in afterload were the main cause for elevated end-diastolic pressures and myocardial fibrosis in ABCG2 KO animals.

It is well accepted that the excess fibrous tissue deposition in the heart is generally due to increased extracellular matrix synthesis and/or proliferation of cardiac fibroblasts (99). We showed that human primary cardiac fibroblasts express ABCG2 and that siRNA against ABCG2 significantly increased their collagen production under hypoxia. This indicates that the results obtained from the mouse model might be relevant for cardiac fibrosis and dysfunction in humans. Fibroblast-mediated matrix production may lead to increased ventricular fibrosis which may result in diastolic dysfunction of the heart and elevated end-diastolic pressure. Therefore, our results could indicate a new molecular mechanism of hypoxia-induced diastolic dysfunction. In contrast, the development of ABCG2 inhibitors is being expedited because ABCG2 provides multidrug resistance for tumour cells by active drug efflux and the bioavailability of anticancer drugs can be improved by co-administration of ABCG2 inhibitors (57,147). Therefore, close attention to the cardiac side effects of this new anticancer strategy is warranted, especially in hypoxemic patients, even if hypoxia is manifest only during night time (e.g. sleep apnea syndrome), and possibly in those with ischemic heart disease.

The present findings suggest that ABCG2 inhibition might cause adverse cardiac effects, if it were to be used in cancer patients. However, the clinical extrapolation of our findings should be done with caution as most of them rely on a mouse model where chronic hypoxia was applied and the human data were based on only one cardiac cell line. Therefore, it is possible that not all these results apply to the human condition. On the other hand it is impossible to test ABCG2 inhibition in humans under hypoxic conditions. In addition, our experimental model employs 4 weeks of constant hypoxia, while in patients, hypoxemia is more often present as an intermittent sleep-associated event. Although the interaction of hypoxia and the lack of ABCG2 showed the same pattern for RVEDP, LVEDP, RV fibrosis, LV fibrosis and human fibroblast collagen production, it did not reach statistical significance for LVEDP. This was most probably due to the small sample size but we cannot exclude that other factors may have played a role.

In conclusion, we provide evidence that loss of ABCG2 under hypoxia leads to biventricular fibrosis and diastolic dysfunction, but does not affect the development of pulmonary hypertension. The use of ABCG2 inhibitors in cancer patients might cause drug-induced cardiotoxicity, particularly in hypoxemic patients or ischemic heart disease.

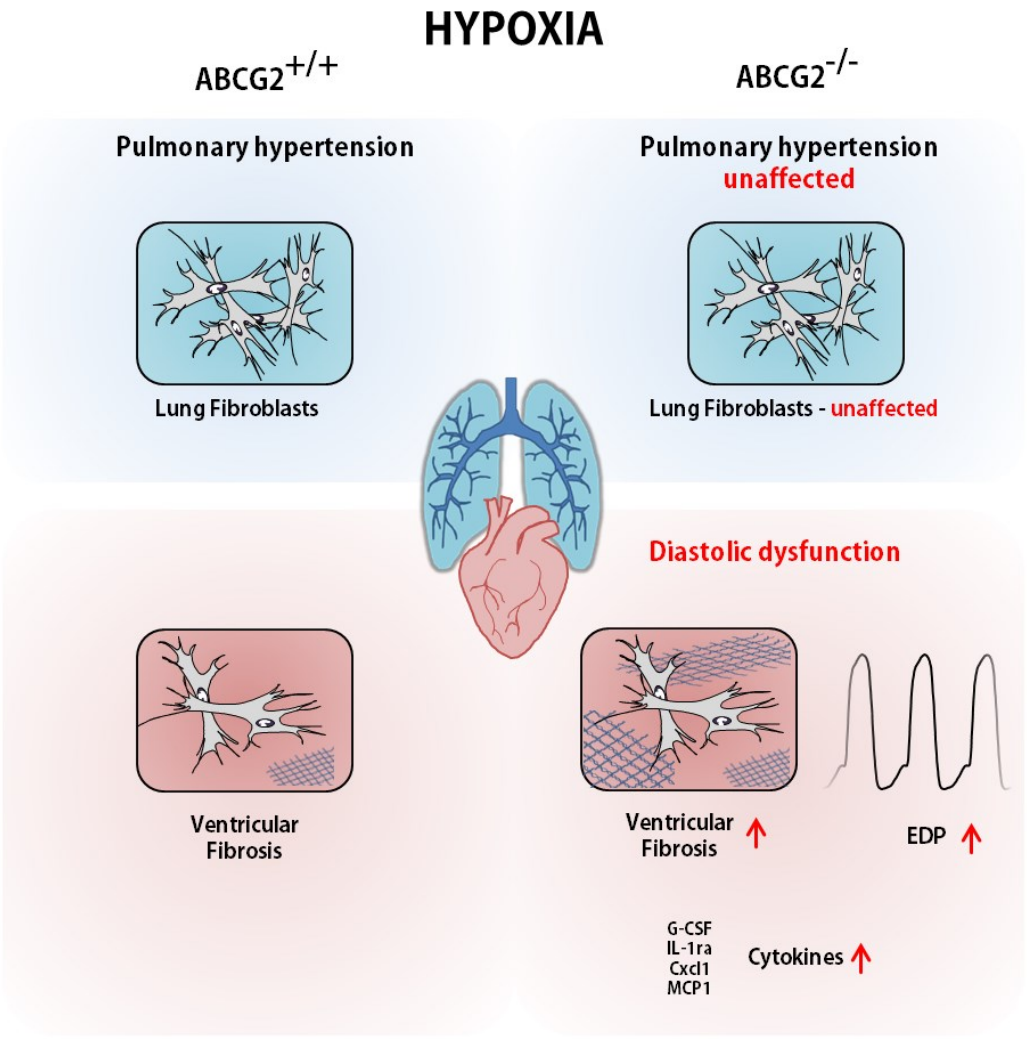

Figure 30. Schematic representation of the findings

The loss of ABCG2 does not influence the development of hypoxia-induced pulmonary hypertension or the extracellular matrix-production of lung fibroblasts. However, in the absence of ABCG2 the cardiac fibroblast-mediated collagen production increases in the heart, accompanied with elevated profibrotic cytokine production. These lead to increased ventricular fibrosis and stiffness, which may result in diastolic dysfunction manifested by elevated end-diastolic pressure.

Bibliography

(1) Sitbon O, Lascoux-Combe C, Delfraissy JF, Yeni PG, Raffi F, De Zuttere D, et al. Prevalence of HIV-related pulmonary arterial hypertension in the current antiretroviral therapy era. Am J Respir Crit Care Med 2008 Jan 1;177(1):108-113.

(2) Hachulla E, Gressin V, Guillevin L, Carpentier P, Diot E, Sibilia J, et al. Early detection of pulmonary arterial hypertension in systemic sclerosis: a French nationwide prospective multicenter study. Arthritis Rheum 2005 Dec;52(12):3792-3800.

(3) Mukerjee D, St George D, Coleiro B, Knight C, Denton CP, Davar J, et al. Prevalence and outcome in systemic sclerosis associated pulmonary arterial hypertension: application of a registry approach. Ann Rheum Dis 2003 Nov;62(11):1088-1093.

(4) Fonseca GH, Souza R, Salemi VM, Jardim CV, Gualandro SF. Pulmonary hypertension diagnosed by right heart catheterisation in sickle cell disease. Eur Respir J 2012 Jan;39(1):112-118.

(5) Peacock AJ, Murphy NF, McMurray JJ, Caballero L, Stewart S. An epidemiological study of pulmonary arterial hypertension. Eur Respir J 2007 Jul;30(1):104-109.

(6) Gaine SP, Rubin LJ. Primary pulmonary hypertension. Lancet 1998 Aug 29;352(9129):719-725.

(7) Badesch DB, Raskob GE, Elliott CG, Krichman AM, Farber HW, Frost AE, et al. Pulmonary arterial hypertension: baseline characteristics from the REVEAL Registry. Chest 2010 Feb;137(2):376-387.

(8) Frost AE, Badesch DB, Barst RJ, Benza RL, Elliott CG, Farber HW, et al. The changing picture of patients with pulmonary arterial hypertension in the United States: how REVEAL differs from historic and non-US Contemporary Registries. Chest 2011 Jan;139(1):128-137.

(9) Rabinovitch M. Molecular pathogenesis of pulmonary arterial hypertension. J Clin Invest 2012 Dec;122(12):4306-4313.

(10) Voelkel NF, Gomez-Arroyo J, Abbate A, Bogaard HJ, Nicolls MR. Pathobiology of pulmonary arterial hypertension and right ventricular failure. Eur Respir J 2012 Dec;40(6):1555-1565.

(11) Guignabert C, Dorfmuller P. Pathology and pathobiology of pulmonary hypertension. Semin Respir Crit Care Med 2013 Oct;34(5):551-559.

(12) Budhiraja R, Tuder RM, Hassoun PM. Endothelial dysfunction in pulmonary hypertension. Circulation 2004 Jan 20;109(2):159-165.

(13) Ward JP, McMurtry IF. Mechanisms of hypoxic pulmonary vasoconstriction and their roles in pulmonary hypertension: new findings for an old problem. Curr Opin Pharmacol 2009 Jun;9(3):287-296.

(14) Leopold JA, Maron BA. Molecular Mechanisms of Pulmonary Vascular Remodeling in Pulmonary Arterial Hypertension. Int J Mol Sci 2016 May 18;17(5):10.3390/ijms17050761.

(15) Austin ED, Loyd JE. The genetics of pulmonary arterial hypertension. Circ Res 2014 Jun 20;115(1):189-202.

(16) Badesch DB, McLaughlin VV, Delcroix M, Vizza CD, Olschewski H, Sitbon O, et al. Prostanoid therapy for pulmonary arterial hypertension. J Am Coll Cardiol 2004 Jun 16;43(12 Suppl S):56S-61S.

(17) Olschewski H. Inhaled iloprost for the treatment of pulmonary hypertension. Eur Respir Rev 2009 Mar;18(111):29-34.

(18) Rubin LJ. Endothelin receptor antagonists for the treatment of pulmonary artery hypertension. Life Sci 2012 Oct 15;91(13-14):517-521.

(19) Galie N, Olschewski H, Oudiz RJ, Torres F, Frost A, Ghofrani HA, et al. Ambrisentan for the treatment of pulmonary arterial hypertension: results of the ambrisentan in pulmonary arterial hypertension, randomized, double-blind, placebo-controlled, multicenter, efficacy (ARIES) study 1 and 2. Circulation 2008 Jun 10;117(23):3010-3019.

(20) Galie N, Brundage BH, Ghofrani HA, Oudiz RJ, Simonneau G, Safdar Z, et al. Tadalafil therapy for pulmonary arterial hypertension. Circulation 2009 Jun 9;119(22):2894-2903.

(21) Rich S, Kaufmann E, Levy PS. The effect of high doses of calcium-channel blockers on survival in primary pulmonary hypertension. N Engl J Med 1992 Jul 9;327(2):76-81.

(22) Chin KM, Kim NH, Rubin LJ. The right ventricle in pulmonary hypertension. Coron Artery Dis 2005 Feb;16(1):13-18.

(23) Vonk Noordegraaf A, Galie N. The role of the right ventricle in pulmonary arterial hypertension. Eur Respir Rev 2011 Dec;20(122):243-253.

(24) Badano LP, Ginghina C, Easaw J, Muraru D, Grillo MT, Lancellotti P, et al. Right ventricle in pulmonary arterial hypertension: haemodynamics, structural changes, imaging, and proposal of a study protocol aimed to assess remodelling and treatment effects. Eur J Echocardiogr 2010 Jan;11(1):27-37.

(25) Bogaard HJ, Abe K, Vonk Noordegraaf A, Voelkel NF. The right ventricle under pressure: cellular and molecular mechanisms of right-heart failure in pulmonary hypertension. Chest 2009 Mar;135(3):794-804.

(26) Haddad F, Ashley E, Michelakis ED. New insights for the diagnosis and management of right ventricular failure, from molecular imaging to targeted right ventricular therapy. Curr Opin Cardiol 2010 Mar;25(2):131-140.

(27) Zimnicka AM, Tang H, Guo Q, Kuhr FK, Oh MJ, Wan J, et al. Upregulated copper transporters in hypoxia-induced pulmonary hypertension. PLoS One 2014 Mar 10;9(3):e90544.

(28) Dempsie Y, Maclean MR. Role of the serotonin transporter in pulmonary arterial hypertension. Expert Rev Clin Pharmacol 2008 Nov;1(6):749-757.

(29) Yuan JX-, Ward JPT, editors. Membrane receptors, channels and transporters in pulmonary circulation. Grover Conference on the Pulmonary Circulation; 2008; Dordrecht: Humana Press; 2010.

(30) Lin T, Islam O, Heese K. ABC transporters, neural stem cells and neurogenesis--a different perspective. Cell Res 2006 Nov;16(11):857-871.

(31) Dean M, Rzhetsky A, Allikmets R. The human ATP-binding cassette (ABC) transporter superfamily. Genome Res 2001 Jul;11(7):1156-1166.

(32) Langmann T, Mauerer R, Zahn A, Moehle C, Probst M, Stremmel W, et al. Real-time reverse transcription-PCR expression profiling of the complete human ATP-binding cassette transporter superfamily in various tissues. Clin Chem 2003 Feb;49(2):230-238.

(33) van der Deen M, de Vries EG, Timens W, Scheper RJ, Timmer-Bosscha H, Postma DS. ATP-binding cassette (ABC) transporters in normal and pathological lung. Respir Res 2005 Jun 20;6:59.

(34) Scheffer GL, Pijnenborg AC, Smit EF, Muller M, Postma DS, Timens W, et al. Multidrug resistance related molecules in human and murine lung. J Clin Pathol 2002 May;55(5):332-339.

(35) Hara Y, Sassi Y, Guibert C, Gambaryan N, Dorfmuller P, Eddahibi S, et al. Inhibition of MRP4 prevents and reverses pulmonary hypertension in mice. J Clin Invest 2011 Jul;121(7):2888-2897.

(36) Mo W, Zhang JT. Human ABCG2: structure, function, and its role in multidrug resistance. Int J Biochem Mol Biol 2012;3(1):1-27.

(37) Maliepaard M, Scheffer GL, Faneyte IF, van Gastelen MA, Pijnenborg AC, Schinkel AH, et al. Subcellular localization and distribution of the breast cancer resistance protein transporter in normal human tissues. Cancer Res 2001 Apr 15;61(8):3458-3464.

(38) Aust S, Obrist P, Jaeger W, Klimpfinger M, Tucek G, Wrba F, et al. Subcellular localization of the ABCG2 transporter in normal and malignant human gallbladder epithelium. Lab Invest 2004 Aug;84(8):1024-1036.

(39) Fetsch PA, Abati A, Litman T, Morisaki K, Honjo Y, Mittal K, et al. Localization of the ABCG2 mitoxantrone resistance-associated protein in normal tissues. Cancer Lett 2006 Apr 8;235(1):84-92.

(40) Huls M, Brown CD, Windass AS, Sayer R, van den Heuvel JJ, Heemskerk S, et al. The breast cancer resistance protein transporter ABCG2 is expressed in the human kidney proximal tubule apical membrane. Kidney Int 2008 Jan;73(2):220-225.

(41) Bailey-Dell KJ, Hassel B, Doyle LA, Ross DD. Promoter characterization and genomic organization of the human breast cancer resistance protein (ATP-binding cassette transporter G2) gene. Biochim Biophys Acta 2001 Sep 21;1520(3):234-241.

(42) Krishnamurthy P, Ross DD, Nakanishi T, Bailey-Dell K, Zhou S, Mercer KE, et al. The stem cell marker Bcrp/ABCG2 enhances hypoxic cell survival through interactions with heme. J Biol Chem 2004 Jun 4;279(23):24218-24225.

(43) Hofer T, Wenger RH, Kramer MF, Ferreira GC, Gassmann M. Hypoxic up-regulation of erythroid 5-aminolevulinate synthase. Blood 2003 Jan 1;101(1):348-350.

(44) Blokhina O, Virolainen E, Fagerstedt KV. Antioxidants, oxidative damage and oxygen deprivation stress: a review. Ann Bot 2003 Jan;91 Spec No:179-194.

(45) Nakanishi T, Ross DD. Breast cancer resistance protein (BCRP/ABCG2): its role in multidrug resistance and regulation of its gene expression. Chin J Cancer 2012 Feb;31(2):73-99.

(46) Szatmari I, Vamosi G, Brazda P, Balint BL, Benko S, Szeles L, et al. Peroxisome proliferator-activated receptor gamma-regulated ABCG2 expression confers cytoprotection to human dendritic cells. J Biol Chem 2006 Aug 18;281(33):23812-23823.

(47) Ee PL, Kamalakaran S, Tonetti D, He X, Ross DD, Beck WT. Identification of a novel estrogen response element in the breast cancer resistance protein (ABCG2) gene. Cancer Res 2004 Feb 15;64(4):1247-1251.

(48) Imai Y, Ishikawa E, Asada S, Sugimoto Y. Estrogen-mediated post transcriptional down-regulation of breast cancer resistance protein/ABCG2. Cancer Res 2005 Jan 15;65(2):596-604.

(49) Wang H, Zhou L, Gupta A, Vethanayagam RR, Zhang Y, Unadkat JD, et al. Regulation of BCRP/ABCG2 expression by progesterone and 17beta-estradiol in human placental BeWo cells. Am J Physiol Endocrinol Metab 2006 May;290(5):E798-807.

(50) Jani M, Ambrus C, Magnan R, Jakab KT, Beery E, Zolnerciks JK, et al. Structure and function of BCRP, a broad specificity transporter of xenobiotics and endobiotics. Arch Toxicol 2014 Apr 29.

(51) Hardwick LJ, Velamakanni S, van Veen HW. The emerging pharmacotherapeutic significance of the breast cancer resistance protein (ABCG2). Br J Pharmacol 2007 May;151(2):163-174.

(52) Zhou S, Morris JJ, Barnes Y, Lan L, Schuetz JD, Sorrentino BP. Bcrp1 gene expression is required for normal numbers of side population stem cells in mice, and confers relative protection to mitoxantrone in hematopoietic cells in vivo. Proc Natl Acad Sci U S A 2002 Sep 17;99(19):12339-12344.

(53) Pfister O, Oikonomopoulos A, Sereti KI, Sohn RL, Cullen D, Fine GC, et al. Role of the ATP-binding cassette transporter Abcg2 in the phenotype and function of cardiac side population cells. Circ Res 2008 Oct 10;103(8):825-835.

(54) Zhou S, Schuetz JD, Bunting KD, Colapietro AM, Sampath J, Morris JJ, et al. The ABC transporter Bcrp1/ABCG2 is expressed in a wide variety of stem cells and is a molecular determinant of the side-population phenotype. Nat Med 2001 Sep;7(9):1028-1034.

(55) Scharenberg CW, Harkey MA, Torok-Storb B. The ABCG2 transporter is an efficient Hoechst 33342 efflux pump and is preferentially expressed by immature human hematopoietic progenitors. Blood 2002 Jan 15;99(2):507-512.

(56) Chow K, Fessel JP, Kaoriihida-Stansbury, Schmidt EP, Gaskill C, Alvarez D, et al. Dysfunctional resident lung mesenchymal stem cells contribute to pulmonary microvascular remodeling. Pulm Circ 2013 Jan;3(1):31-49.

(57) Wu CP, Calcagno AM, Ambudkar SV. Reversal of ABC drug transporter-mediated multidrug resistance in cancer cells: evaluation of current strategies. Curr Mol Pharmacol 2008 Jun;1(2):93-105.

(58) Szakacs G, Paterson JK, Ludwig JA, Booth-Genthe C, Gottesman MM. Targeting multidrug resistance in cancer. Nat Rev Drug Discov 2006 Mar;5(3):219-234.

(59) Perego P, De Cesare M, De Isabella P, Carenini N, Beggiolin G, Pezzoni G, et al. A novel 7-modified camptothecin analog overcomes breast cancer resistance protein-associated resistance in a mitoxantrone-selected colon carcinoma cell line. Cancer Res 2001 Aug 15;61(16):6034-6037.

(60) Miyake K, Mickley L, Litman T, Zhan Z, Robey R, Cristensen B, et al. Molecular cloning of cDNAs which are highly overexpressed in mitoxantrone-resistant cells: demonstration of homology to ABC transport genes. Cancer Res 1999 Jan 1;59(1):8-13.

(61) Kawabata S, Oka M, Shiozawa K, Tsukamoto K, Nakatomi K, Soda H, et al. Breast cancer resistance protein directly confers SN-38 resistance of lung cancer cells. Biochem Biophys Res Commun 2001 Feb 9;280(5):1216-1223.

(62) Nagashima S, Soda H, Oka M, Kitazaki T, Shiozawa K, Nakamura Y, et al. BCRP/ABCG2 levels account for the resistance to topoisomerase I inhibitors and reversal effects by gefitinib in non-small cell lung cancer. Cancer Chemother Pharmacol 2006 Nov;58(5):594-600.

(63) Maliepaard M, van Gastelen MA, de Jong LA, Pluim D, van Waardenburg RC, Ruevekamp-Helmers MC, et al. Overexpression of the BCRP/MXR/ABCP gene in a topotecan-selected ovarian tumor cell line. Cancer Res 1999 Sep 15;59(18):4559-4563.

(64) Stein U, Lage H, Jordan A, Walther W, Bates SE, Litman T, et al. Impact of BCRP/MXR, MRP1 and MDR1/P-Glycoprotein on thermoresistant variants of atypical and classical multidrug resistant cancer cells. Int J Cancer 2002 Feb 20;97(6):751-760.

(65) Turner JG, Gump JL, Zhang C, Cook JM, Marchion D, Hazlehurst L, et al. ABCG2 expression, function, and promoter methylation in human multiple myeloma. Blood 2006 Dec 1;108(12):3881-3889.

(66) Kamiyama N, Takagi S, Yamamoto C, Kudo T, Nakagawa T, Takahashi M, et al. Expression of ABC transporters in human hepatocyte carcinoma cells with cross-resistance to epirubicin and mitoxantrone. Anticancer Res 2006 Mar-Apr;26(2A):885-888.

(67) van Herwaarden AE, Schinkel AH. The function of breast cancer resistance protein in epithelial barriers, stem cells and milk secretion of drugs and xenotoxins. Trends Pharmacol Sci 2006 Jan;27(1):10-16.

(68) Mao Q. BCRP/ABCG2 in the placenta: expression, function and regulation. Pharm Res 2008 Jun;25(6):1244-1255.

(69) Enokizono J, Kusuhara H, Ose A, Schinkel AH, Sugiyama Y. Quantitative investigation of the role of breast cancer resistance protein (Bcrp/Abcg2) in limiting brain and testis penetration of xenobiotic compounds. Drug Metab Dispos 2008 Jun;36(6):995-1002.

(70) Breedveld P, Pluim D, Cipriani G, Wielinga P, van Tellingen O, Schinkel AH, et al. The effect of Bcrp1 (Abcg2) on the in vivo pharmacokinetics and brain penetration of imatinib mesylate (Gleevec): implications for the use of breast cancer resistance protein and P-glycoprotein inhibitors to enable the brain penetration of imatinib in patients. Cancer Res 2005 Apr 1;65(7):2577-2582.

(71) Pick A, Klinkhammer W, Wiese M. Specific inhibitors of the breast cancer resistance protein (BCRP). ChemMedChem 2010 Sep 3;5(9):1498-1505.

(72) Jonker JW, Smit JW, Brinkhuis RF, Maliepaard M, Beijnen JH, Schellens JH, et al. Role of breast cancer resistance protein in the bioavailability and fetal penetration of topotecan. J Natl Cancer Inst 2000 Oct 18;92(20):1651-1656.

(73) Kuppens IE, Witteveen EO, Jewell RC, Radema SA, Paul EM, Mangum SG, et al. A phase I, randomized, open-label, parallel-cohort, dose-finding study of elacridar (GF120918) and oral topotecan in cancer patients. Clin Cancer Res 2007 Jun 1;13(11):3276-3285.

(74) Kruijtzer CM, Beijnen JH, Rosing H, ten Bokkel Huinink WW, Schot M, Jewell RC, et al. Increased oral bioavailability of topotecan in combination with the breast cancer resistance protein and P-glycoprotein inhibitor GF120918. J Clin Oncol 2002 Jul 1;20(13):2943-2950.

(75) Chuan Tang S, Nguyen LN, Sparidans RW, Wagenaar E, Beijnen JH, Schinkel AH. Increased oral availability and brain accumulation of the ALK inhibitor crizotinib by coadministration of the P-glycoprotein (ABCB1) and breast cancer resistance protein (ABCG2) inhibitor elacridar. Int J Cancer 2014 Mar 15;134(6):1484-1494.

(76) Beltrami AP, Barlucchi L, Torella D, Baker M, Limana F, Chimenti S, et al. Adult cardiac stem cells are multipotent and support myocardial regeneration. Cell 2003 Sep 19;114(6):763-776.

(77) Sereti KI, Oikonomopoulos A, Unno K, Cao X, Qiu Y, Liao R. ATP-binding cassette G-subfamily transporter 2 regulates cell cycle progression and asymmetric division in mouse cardiac side population progenitor cells. Circ Res 2013 Jan 4;112(1):27-34.

(78) Meissner K, Heydrich B, Jedlitschky G, Meyer Zu Schwabedissen H, Mosyagin I, Dazert P, et al. The ATP-binding cassette transporter ABCG2 (BCRP), a marker for side population stem cells, is expressed in human heart. J Histochem Cytochem 2006 Feb;54(2):215-221.

(79) Solbach TF, Paulus B, Weyand M, Eschenhagen T, Zolk O, Fromm MF. ATP-binding cassette transporters in human heart failure. Naunyn Schmiedebergs Arch Pharmacol 2008 May;377(3):231-243.

(80) Higashikuni Y, Sainz J, Nakamura K, Takaoka M, Enomoto S, Iwata H, et al. The ATP-binding cassette transporter ABCG2 protects against pressure overload-induced cardiac

hypertrophy and heart failure by promoting angiogenesis and antioxidant response. Arterioscler Thromb Vasc Biol 2012 Mar;32(3):654-661.

(81) Higashikuni Y, Sainz J, Nakamura K, Takaoka M, Enomoto S, Iwata H, et al. The ATP-binding cassette transporter BCRP1/ABCG2 plays a pivotal role in cardiac repair after myocardial infarction via modulation of microvascular endothelial cell survival and function. Arterioscler Thromb Vasc Biol 2010 Nov;30(11):2128-2135.

(82) Gaasch WH, Zile MR. Left ventricular diastolic dysfunction and diastolic heart failure. Annu Rev Med 2004;55:373-394.

(83) Larsen KO, Sjaastad I, Svindland A, Krobert KA, Skjonsberg OH, Christensen G. Alveolar hypoxia induces left ventricular diastolic dysfunction and reduces phosphorylation of phospholamban in mice. Am J Physiol Heart Circ Physiol 2006 Aug;291(2):H507-16.

(84) Burlew BS, Weber KT. Cardiac fibrosis as a cause of diastolic dysfunction. Herz 2002 Mar;27(2):92-98.

(85) Zile MR, Brutsaert DL. New concepts in diastolic dysfunction and diastolic heart failure: Part I: diagnosis, prognosis, and measurements of diastolic function. Circulation 2002 Mar 19;105(11):1387-1393.

(86) Tian R, Nascimben L, Ingwall JS, Lorell BH. Failure to maintain a low ADP concentration impairs diastolic function in hypertrophied rat hearts. Circulation 1997 Aug 19;96(4):1313-1319.

(87) Zile MR, Baicu CF, Gaasch WH. Diastolic heart failure--abnormalities in active relaxation and passive stiffness of the left ventricle. N Engl J Med 2004 May 6;350(19):1953-1959.

(88) Kovacs G, Olschewski A, Berghold A, Olschewski H. Pulmonary vascular resistances during exercise in normal subjects: a systematic review. Eur Respir J 2012 Feb;39(2):319-328.

(89) Paulus WJ, Tschope C, Sanderson JE, Rusconi C, Flachskampf FA, Rademakers FE, et al. How to diagnose diastolic heart failure: a consensus statement on the diagnosis of heart failure with normal left ventricular ejection fraction by the Heart Failure and Echocardiography Associations of the European Society of Cardiology. Eur Heart J 2007 Oct;28(20):2539-2550.

(90) Martos R, Baugh J, Ledwidge M, O'Loughlin C, Conlon C, Patle A, et al. Diastolic heart failure: evidence of increased myocardial collagen turnover linked to diastolic dysfunction. Circulation 2007 Feb 20;115(7):888-895.

(91) Chiao YA, Ramirez TA, Zamilpa R, Okoronkwo SM, Dai Q, Zhang J, et al. Matrix metalloproteinase-9 deletion attenuates myocardial fibrosis and diastolic dysfunction in ageing mice. Cardiovasc Res 2012 Dec 1;96(3):444-455.

(92) Chaturvedi RR, Herron T, Simmons R, Shore D, Kumar P, Sethia B, et al. Passive stiffness of myocardium from congenital heart disease and implications for diastole. Circulation 2010 Mar 2;121(8):979-988.

(93) Robinson TF, Geraci MA, Sonnenblick EH, Factor SM. Coiled perimysial fibers of papillary muscle in rat heart: morphology, distribution, and changes in configuration. Circ Res 1988 Sep;63(3):577-592.

(94) Weber KT, Sun Y, Bhattacharya SK, Ahokas RA, Gerling IC. Myofibroblast-mediated mechanisms of pathological remodelling of the heart. Nat Rev Cardiol 2013 Jan;10(1):15-26.

(95) Weber KT, Brilla CG, Janicki JS. Myocardial fibrosis: functional significance and regulatory factors. Cardiovasc Res 1993 Mar;27(3):341-348.

(96) Kuwahara F, Kai H, Tokuda K, Takeya M, Takeshita A, Egashira K, et al. Hypertensive myocardial fibrosis and diastolic dysfunction: another model of inflammation? Hypertension 2004 Apr;43(4):739-745.

(97) van Heerebeek L, Hamdani N, Handoko ML, Falcao-Pires I, Musters RJ, Kupreishvili K, et al. Diastolic stiffness of the failing diabetic heart: importance of fibrosis, advanced glycation end products, and myocyte resting tension. Circulation 2008 Jan 1;117(1):43-51.

(98) Souders CA, Bowers SL, Baudino TA. Cardiac fibroblast: the renaissance cell. Circ Res 2009 Dec 4;105(12):1164-1176.

(99) Camelliti P, Borg TK, Kohl P. Structural and functional characterisation of cardiac fibroblasts. Cardiovasc Res 2005 Jan 1;65(1):40-51.

(100) Jonker JW, Buitelaar M, Wagenaar E, Van Der Valk MA, Scheffer GL, Scheper RJ, et al. The breast cancer resistance protein protects against a major chlorophyll-derived dietary phototoxin and protoporphyria. Proc Natl Acad Sci U S A 2002 Nov 26;99(24):15649-15654.

(101) Nagaraj C, Tang B, Nagy BM, Papp R, Jain PP, Marsh LM, et al. Docosahexaenoic acid causes rapid pulmonary arterial relaxation via KCa channel-mediated hyperpolarisation in pulmonary hypertension. Eur Respir J 2016 Oct;48(4):1127-1136.

(102) Nagy BM, Nagaraj C, Egemnazarov B, Kwapiszewska G, Stauber RE, Avian A, et al. Lack of ABCG2 Leads to Biventricular Dysfunction and Remodeling in Response to Hypoxia. Front Physiol 2017 Feb 21;8:98.

(103) Egemnazarov B, Schmidt A, Crnkovic S, Sydykov A, Nagy BM, Kovacs G, et al. Pressure Overload Creates Right Ventricular Diastolic Dysfunction in a Mouse Model: Assessment by Echocardiography. J Am Soc Echocardiogr 2015 Jul;28(7):828-843.

(104) Perros F, Montani D, Dorfmuller P, Durand-Gasselin I, Tcherakian C, Le Pavec J, et al. Platelet-derived growth factor expression and function in idiopathic pulmonary arterial hypertension. Am J Respir Crit Care Med 2008 Jul 1;178(1):81-88.

(105) Heldin CH, Westermark B. Mechanism of action and in vivo role of platelet-derived growth factor. Physiol Rev 1999 Oct;79(4):1283-1316.

(106) Juvale K, Pape VF, Wiese M. Investigation of chalcones and benzochalcones as inhibitors of breast cancer resistance protein. Bioorg Med Chem 2012 Jan 1;20(1):346-355.

(107) Stacey DW. Cyclin D1 serves as a cell cycle regulatory switch in actively proliferating cells. Curr Opin Cell Biol 2003 Apr;15(2):158-163.

(108) Crnkovic S, Hrzenjak A, Marsh LM, Olschewski A, Kwapiszewska G. Origin of neomuscularized vessels in mice exposed to chronic hypoxia. Respir Physiol Neurobiol 2011 Dec 15;179(2-3):342-345.

(109) Leslie EM, Deeley RG, Cole SP. Multidrug resistance proteins: role of P-glycoprotein, MRP1, MRP2, and BCRP (ABCG2) in tissue defense. Toxicol Appl Pharmacol 2005 May 1;204(3):216-237.

(110) Rubin LJ, Handel F, Peter RH. The effects of oral hydralazine on right ventricular end-diastolic pressure in patients with right ventricular failure. Circulation 1982 Jun;65(7):1369-1373.

(111) Schafer S, Ellinghaus P, Janssen W, Kramer F, Lustig K, Milting H, et al. Chronic inhibition of phosphodiesterase 5 does not prevent pressure-overload-induced right-ventricular remodelling. Cardiovasc Res 2009 Apr 1;82(1):30-39.

(112) Hameed AG, Arnold ND, Chamberlain J, Pickworth JA, Paiva C, Dawson S, et al. Inhibition of tumor necrosis factor-related apoptosis-inducing ligand (TRAIL) reverses experimental pulmonary hypertension. J Exp Med 2012 Oct 22;209(11):1919-1935.

(113) Urashima T, Zhao M, Wagner R, Fajardo G, Farahani S, Quertermous T, et al. Molecular and physiological characterization of RV remodeling in a murine model of pulmonary stenosis. Am J Physiol Heart Circ Physiol 2008 Sep;295(3):H1351-H1368.

(114) Greyson C, Xu Y, Cohen J, Schwartz GG. Right ventricular dysfunction persists following brief right ventricular pressure overload. Cardiovasc Res 1997 May;34(2):281-288.

(115) Angelini DJ, Su Q, Yamaji-Kegan K, Fan C, Skinner JT, Champion HC, et al. Hypoxia-induced mitogenic factor (HIMF/FIZZ1/RELMalpha) induces the vascular and hemodynamic changes of pulmonary hypertension. Am J Physiol Lung Cell Mol Physiol 2009 Apr;296(4):L582-93.

(116) Rain S, Handoko ML, Trip P, Gan CT, Westerhof N, Stienen GJ, et al. Right ventricular diastolic impairment in patients with pulmonary arterial hypertension. Circulation 2013 Oct 29;128(18):2016-25, 1-10.

(117) Tomanek RJ. Response of the coronary vasculature to myocardial hypertrophy. J Am Coll Cardiol 1990 Mar 1;15(3):528-533.

(118) Kessler R, Chaouat A, Weitzenblum E, Oswald M, Ehrhart M, Apprill M, et al. Pulmonary hypertension in the obstructive sleep apnoea syndrome: prevalence, causes and therapeutic consequences. Eur Respir J 1996 Apr;9(4):787-794.

(119) Laveneziana P, Garcia G, Joureau B, Nicolas-Jilwan F, Brahimi T, Laviolette L, et al. Dynamic respiratory mechanics and exertional dyspnoea in pulmonary arterial hypertension. Eur Respir J 2013 Mar;41(3):578-587.

(120) Campos-Rodriguez F, Martinez-Garcia MA, Martinez M, Duran-Cantolla J, Pena Mde L, Masdeu MJ, et al. Association between obstructive sleep apnea and cancer incidence in a large multicenter Spanish cohort. Am J Respir Crit Care Med 2013 Jan 1;187(1):99-105.

(121) Nieto FJ, Peppard PE, Young T, Finn L, Hla KM, Farre R. Sleep-disordered breathing and cancer mortality: results from the Wisconsin Sleep Cohort Study. Am J Respir Crit Care Med 2012 Jul 15;186(2):190-194.

(122) Maarman G, Lecour S, Butrous G, Thienemann F, Sliwa K. A comprehensive review: the evolution of animal models in pulmonary hypertension research; are we there yet? Pulm Circ 2013 Dec;3(4):739-756.

(123) Stenmark KR, Meyrick B, Galie N, Mooi WJ, McMurtry IF. Animal models of pulmonary arterial hypertension: the hope for etiological discovery and pharmacological cure. Am J Physiol Lung Cell Mol Physiol 2009 Dec;297(6):L1013-32.

(124) Ryan J, Bloch K, Archer SL. Rodent models of pulmonary hypertension: harmonisation with the world health organisation's categorisation of human PH. Int J Clin Pract Suppl 2011 Aug;(172):15-34. doi(172):15-34.

(125) Humbert M, Morrell NW, Archer SL, Stenmark KR, MacLean MR, Lang IM, et al. Cellular and molecular pathobiology of pulmonary arterial hypertension. J Am Coll Cardiol 2004 Jun 16;43(12 Suppl S):13S-24S.

(126) van de Veerdonk MC, Kind T, Marcus JT, Mauritz GJ, Heymans MW, Bogaard HJ, et al. Progressive right ventricular dysfunction in patients with pulmonary arterial hypertension responding to therapy. J Am Coll Cardiol 2011 Dec 6;58(24):2511-2519.

(127) Leite-Moreira AF, Correia-Pinto J, Gillebert TC. Afterload induced changes in myocardial relaxation: a mechanism for diastolic dysfunction. Cardiovasc Res 1999 Aug 1;43(2):344-353.

(128) Salem R, Denault AY, Couture P, Belisle S, Fortier A, Guertin MC, et al. Left ventricular end-diastolic pressure is a predictor of mortality in cardiac surgery independently of left ventricular ejection fraction. Br J Anaesth 2006 Sep;97(3):292-297.

(129) Emmert MY, Emmert LS, Martens A, Ismail I, Schmidt-Richter I, Gawol A, et al. Higher frequencies of BCRP+ cardiac resident cells in ischaemic human myocardium. Eur Heart J 2013 Sep;34(36):2830-2838.

(130) Unno K, Jain M, Liao R. Cardiac side population cells: moving toward the center stage in cardiac regeneration. Circ Res 2012 May 11;110(10):1355-1363.

(131) Periasamy M, Huke S. SERCA pump level is a critical determinant of Ca(2+)homeostasis and cardiac contractility. J Mol Cell Cardiol 2001 Jun;33(6):1053-1063.

(132) del Monte F, Harding SE, Dec GW, Gwathmey JK, Hajjar RJ. Targeting phospholamban by gene transfer in human heart failure. Circulation 2002 Feb 26;105(8):904-907.

(133) del Monte F, Hajjar RJ. Targeting calcium cycling proteins in heart failure through gene transfer. J Physiol 2003 Jan 1;546(Pt 1):49-61.

(134) Armoundas AA, Hobai IA, Tomaselli GF, Winslow RL, O'Rourke B. Role of sodium-calcium exchanger in modulating the action potential of ventricular myocytes from normal and failing hearts. Circ Res 2003 Jul 11;93(1):46-53.

(135) Weber CR, Piacentino V,3rd, Houser SR, Bers DM. Dynamic regulation of sodium/calcium exchange function in human heart failure. Circulation 2003 Nov 4;108(18):2224-2229.

(136) Kass DA, Bronzwaer JG, Paulus WJ. What mechanisms underlie diastolic dysfunction in heart failure? Circ Res 2004 Jun 25;94(12):1533-1542.

(137) Angeja BG, Grossman W. Evaluation and management of diastolic heart failure. Circulation 2003 Feb 11;107(5):659-663.

(138) MacKenna DA, Omens JH, McCulloch AD, Covell JW. Contribution of collagen matrix to passive left ventricular mechanics in isolated rat hearts. Am J Physiol 1994 Mar;266(3 Pt 2):H1007-18.

(139) Brilla CG, Funck RC, Rupp H. Lisinopril-mediated regression of myocardial fibrosis in patients with hypertensive heart disease. Circulation 2000 Sep 19;102(12):1388-1393.

(140) Querejeta R, Varo N, Lopez B, Larman M, Artinano E, Etayo JC, et al. Serum carboxy-terminal propeptide of procollagen type I is a marker of myocardial fibrosis in hypertensive heart disease. Circulation 2000 Apr 11;101(14):1729-1735.

(141) Moreo A, Ambrosio G, De Chiara B, Pu M, Tran T, Mauri F, et al. Influence of myocardial fibrosis on left ventricular diastolic function: noninvasive assessment by cardiac magnetic resonance and echo. Circ Cardiovasc Imaging 2009 Nov;2(6):437-443.

(142) Muller-Brunotte R, Kahan T, Lopez B, Edner M, Gonzalez A, Diez J, et al. Myocardial fibrosis and diastolic dysfunction in patients with hypertension: results from the Swedish Irbesartan Left Ventricular Hypertrophy Investigation versus Atenolol (SILVHIA). J Hypertens 2007 Sep;25(9):1958-1966.

(143) Murdoch CE, Chaubey S, Zeng L, Yu B, Ivetic A, Walker SJ, et al. Endothelial NADPH oxidase-2 promotes interstitial cardiac fibrosis and diastolic dysfunction through proinflammatory effects and endothelial-mesenchymal transition. J Am Coll Cardiol 2014 Jun 24;63(24):2734-2741.

(144) Reed AL, Tanaka A, Sorescu D, Liu H, Jeong EM, Sturdy M, et al. Diastolic dysfunction is associated with cardiac fibrosis in the senescence-accelerated mouse. Am J Physiol Heart Circ Physiol 2011 Sep;301(3):H824-31.

(145) Krenning G, Zeisberg EM, Kalluri R. The origin of fibroblasts and mechanism of cardiac fibrosis. J Cell Physiol 2010 Nov;225(3):631-637.

(146) Diez J, Querejeta R, Lopez B, Gonzalez A, Larman M, Martinez Ubago JL. Losartan-dependent regression of myocardial fibrosis is associated with reduction of left ventricular chamber stiffness in hypertensive patients. Circulation 2002 May 28;105(21):2512-2517.

(147) Breedveld P, Beijnen JH, Schellens JH. Use of P-glycoprotein and BCRP inhibitors to improve oral bioavailability and CNS penetration of anticancer drugs. Trends Pharmacol Sci 2006 Jan;27(1):17-24.

Footnotes

The results of the current thesis are published as follows:

Lack of ABCG2 Leads to Biventricular Dysfunction and Remodeling in Response to Hypoxia
Bence M. Nagy, Chandran Nagaraj, Bakytbek Egemnazarov, Grazyna Kwapiszewska, Rudolf E. Stauber, Alexander Avian, Horst Olschewski and Andrea Olschewski
(Journal Frontiers in Physiology, 2017)

Parts of this dissertation is published in the above original research article, as well parts of the published work are being reproduced in this dissertation.

Presentations:

Lack of ABCG2 leads to biventricular dysfunction and remodelling in response to hypoxia
Bence M. Nagy
(LBG Healthcare, Wien, Austria, 2014)

Poster Presentations:

Enhanced right ventricular diastolic dysfunction in ABCG2 knockout mouse
Bence M. Nagy, Chandran Nagaraj, Grazyna Kwapiszewska, Andrea Olschewski, Horst Olschewski
(American Heart Association, Dallas, USA, 2013)

Loss of ABCG2 leads to right ventricular diastolic dysfunction in pulmonary hypertension
Bence M. Nagy, Chandran Nagaraj, Grazyna Kwapiszewska, Andrea Olschewski, Horst Olschewski
(PneumoUpdate, Innsbruck, Austria, 2013)

Lack of ABCG2 leads to biventricular dysfunction and remodelling in response to hypoxia
Bence M. Nagy, Chandran Nagaraj, Bakytbek Egemnazarov, Grazyna Kwapiszewska, Rudolf E. Stauber, Alexander Avian, Andrea Olschewski, Horst Olschewski

(American Thoracic Society, San Francisco, USA, 2016)